Earth-Science Reviews 258 (2024) 104936

Contents lists available at ScienceDirect

Earth-Science Reviews

journal homepage: www.elsevier.com/locate/earscirev

Glacial erosion and Quaternary landscape development of the Eurasian Arctic

Henry Patton [a,*], Nikolitsa Alexandropoulou [b], Amando P.E. Lasabuda [b,c,d], Jochen Knies [a,e], Karin Andreassen [b], Monica Winsborrow [a], Jan Sverre Laberg [b], Alun Hubbard [a,f]

[a] iC3: Centre for ice, Cryosphere, Carbon and Climate, Department of Geosciences, UiT The Arctic University of Norway, N-9037 Tromsø, Norway
[b] Department of Geosciences, UiT The Arctic University of Norway, N-9037 Tromsø, Norway
[c] Centre for Planetary Habitability (PHAB), Department of Geosciences, University of Oslo, Oslo, Norway
[d] EarthByte Group, School of Geosciences, The University of Sydney, Sydney, Australia
[e] Geological Survey of Norway, NO-7491 Trondheim, Norway
[f] Geography Research Unit, University of Oulu, Oulu, Finland

ARTICLE INFO

Keywords:
Quaternary
Erosion
Ice sheet
Landscape evolution
Uplift
Modelling
Barents Shelf
Palaeo topography
Glaciation
Trough mouth fan
Barents Seaway

ABSTRACT

Multiple ice age cycles spanning the last three million years have fundamentally transformed the Arctic landscape. The cadence and intensity of this glacial modification underpin the stability of Arctic geosystems over geologic time scales, including its hydrology, circulation patterns, slope stability, hydrocarbon fluid flow, geochemical/sediment cycling and nutrient supply. The Barents Shelf provides a unique arena to investigate long-term landscape evolution as it has undergone significant glacial modification during the Quaternary and has an extensive stratigraphic data repository motivated by decades of hydrocarbon seismic and well exploration. Here, we assimilate new geological datasets with ice sheet erosion modelling to incrementally reconstruct the geomorphic evolution of the Eurasian Arctic domain over each of the 47 glaciations since the intensification of Northern Hemisphere glaciation ~2.74 Ma. We utilise this time-transgressive framework to review hypotheses regarding the heterogenous development of the Barents Shelf and the timing of key topographic reconfiguration episodes. Our results demonstrate that up to 2.6 km of bedrock was glacially removed to the shelf margins, and though the mean rate of erosion declines over the Quaternary, the efficacy of glacial erosion has a more complex timeline. Initially, erosion was highly effective as large expanses of the Eurasian Arctic switched from subaerial exposure to marine conditions around 2 Ma. Thereafter, erosional efficacy decreased as the landscape desensitised to successive glaciations but, after 1 Ma, it increased as a dynamic, marine-based ice sheet drained by ice streams expanded, selectively eroding large outlet troughs to the shelf edge. Critically for Arctic climate, at ~0.69 Ma this episode of enhanced preferential erosion opened up the Barents Seaway establishing a new circulation pathway between the Atlantic and Arctic Oceans. Our 4D landscape reconstruction provides key boundary conditions for paleoclimate models and establishes a new framework for assessing the profound impact of late-Cenozoic glaciation on the Eurasian Arctic landscape.

1. Introduction

The intensification of large-scale Northern Hemisphere glaciations (NHG) ~2.74 million years ago (Ma) during the late Pliocene instigated major transformations to the Eurasian and North American continental landmasses and their adjoining shelves. As ice sheets waxed and waned, intensive periods of erosion associated with 47 distinct glacial-interglacial cycles resulted in net topographic relief change that exceeded ±1500 m in some areas (Laberg et al., 2012; Medvedev et al., 2018). This glacial-driven modification of the Arctic landscape and associated glacial-isostatic adjustments had profound consequences for global ocean circulation and palaeo-climate (Knudson and Ravelo, 2015; Lasabuda et al., 2023), excavated vast fluxes of bedrock and sediment (Steer et al., 2012; Vorren et al., 1991) and, along with it, mobilised nutrients, geological hydrocarbons and gas hydrates (Serov et al., 2023; Wu et al., 2022).

The erosion and uplift of the Barents Shelf, which today is largely sub-marine with an average water depth of ~184 m, has received

* Corresponding author.
E-mail address: henry.patton@uit.no (H. Patton).

https://doi.org/10.1016/j.earscirev.2024.104936
Received 2 May 2024; Received in revised form 6 September 2024; Accepted 16 September 2024
Available online 19 September 2024
0012-8252/© 2024 The Author(s). Published by Elsevier B.V. This is an open access article under the CC BY license (http://creativecommons.org/licenses/by/4.0/).

considerable attention, in particular, motivated by its setting as a sedimentary basin holding significant petroleum potential (Faleide et al., 1996; Laberg et al., 2010; Løseth et al., 1993; Løtveit et al., 2019; Rasmussen and Fjeldskaar, 1996; Riis and Fjeldskaar, 1992; Vorren et al., 1991; Zieba et al., 2017). Abundant data from areas south of the sea-ice limit has yielded varying levels of insight and stratigraphic control on the topographic evolution of the region and its glacial history (Hjelstuen and Sejrup, 2021; Lasabuda et al., 2021). However, due to both physical and political barriers, large spatial and temporal data gaps remain that require significant levels of interpolation and speculation, resulting in reduced confidence in interpretations at the regional scale.

Of particular interest within this research topic are the trough-mouth fans (TMFs) that lie adjacent to the formerly glaciated shelf in the deep ocean (Fig. 1a). These immense sediment depocentres reflect the incremental erosion and removal of the terrestrial landscape to the adjacent continental slope over million-year timescales, and in some areas have accumulated to over 3 km thick (Faleide et al., 2024; Hjelstuen and Sejrup, 2021; Pope et al., 2018). Such sequences thus represent valuable archives for constraining long-term landscape evolution and sediment source-to-sink processes (Gales et al., 2019), with the changing patterns of deposition recorded within them regularly used to infer the past evolution of ice sheets and their erosional signature across the continental hinterland (Fiedler and Faleide, 1996; Knies et al., 2009; Laberg et al., 2010; Lien et al., 2022).

In this paper, we collate up-to-date knowledge from this sedimentary archive to develop an empirically constrained modelling framework and refine a new glacial landscape evolution model for the Northern Fennoscandian - Barents Sea – Eurasian Arctic domain spanning the late Plio-Pleistocene. This process-based, glaciologically consistent approach delivers a palaeo-landscape reconstruction at an unprecedented temporal and spatial resolution and, with it, essential context to assess existing hypotheses on the development of the Barents Shelf, inform where the largest uncertainties are expected, and where further data collection will be most valuable.

Specifically, we aim to:

i. Review the current state of research into glacial-related uplift and erosion on the Barents Shelf during the late Plio-Pleistocene and its relevance for the wider Arctic environment,
ii. refine volume estimates of the major glacial sediment packages within the Bear Island TMF – the largest depocentre in the Eurasian Arctic,
iii. reconstruct the detailed geomorphic evolution of the Barents Shelf topography at each of the 47 individual glaciations spanning the last 2.74 Ma, and
iv. resolve and discuss the implications of this reconstructed palaeotopography on the Eurasian Arctic especially, and for long-term landscape evolution more generally.

2. Geologic setting

2.1. Chronological terminology

Reference to geological units and age boundaries in this review follows the geologic time scale of the International Commission on Stratigraphy (Cohen et al., 2013; v. 2023/09). The Cenozoic is the current geological era, spanning the last 66 million years of Earth's history. The three most recent epochs within the Cenozoic include the Pliocene (5.333 Ma to 2.58 Ma), Pleistocene (~2.58 Ma to 11.7 ka), and our current interglacial the Holocene (<11.7 ka). While the Quaternary

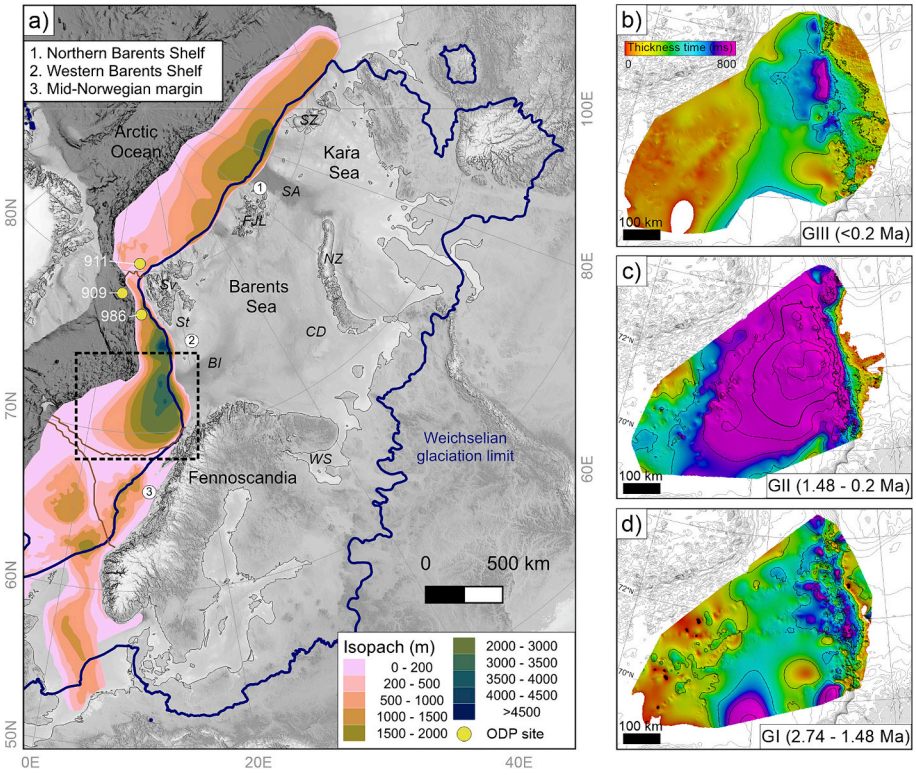

Fig. 1. a) Quaternary isopach map and major offshore sediment depocentres of the Barents and Fennoscandian ice sheets (Hjelstuen and Sejrup, 2021). The Weichselian (<115 ka) glacial maximum shown as a thick blue line represents an amalgamation of peak glacial limits during MIS 2, 4 and 5d, as defined by Batchelor et al. (2019). b-d) Isopach maps of the major glacial units in the Bear Island trough mouth fan (TMF), revised from Alexandropoulou et al. (2021). Name abbreviations: BI – Bear Island Trough; CD – Central deep; FJL – Franz Josef Land; NZ – Novaya Zemlya; SA – Saint Anna Trough; St – Storfjorden Trough; Sv – Svalbard; SZ – Severnaya Zemlya; WS – White Sea. Base topography: The GEBCO_2022 Grid. (For interpretation of the references to colour in this figure legend, the reader is referred to the web version of this article.)

period (<2.58 Ma) – synonymous with glacial-interglacial cycles – spans these two most recent epochs, the focus of this review and modelling framework extends beyond the Quaternary, to the intensification of NHG and transition to an icehouse world within the late Pliocene at ~2.74 Ma, herein referred to as the late Plio-Pleistocene

2.2. The late Pliocene intensification of Northern Hemisphere glaciations

The late Plio-Pleistocene period is characterised by a succession of glacial-interglacial cycles, wherein kilometre-thick ice sheets repeatedly extended across the Arctic. However, this transition from a greenhouse to an icehouse world was likely gradual between 3.6 Ma and 2.4 Ma (Clark et al., 2024; Mudelsee and Raymo, 2005; Raymo, 1994), as inferred from the long-term record of ice-rafted debris (IRD) discharge found at North Atlantic ODP (Ocean Drilling Programme) sites (e.g., Fig. 2).

One potential driver suggested for the onset of NHG at 3.6 Ma is the approximate coeval closure of the Central American Seaways, which gradually terminated water exchange between the Pacific and Atlantic oceans (Bartoli et al., 2005; Haug and Tiedemann, 1998; O'Dea et al., 2016; Öğretmen et al., 2020). It is argued the event enhanced the advection of warm, saline water to northern high latitudes, increasing North Atlantic Deep Water production, which in turn fuelled higher evaporation and increased precipitation over Greenland and Europe (De Schepper et al., 2015; Hayashi et al., 2020; Keigwin, 1982). An alternative, or contributing, hypothesis is that decreasing atmospheric CO_2 concentrations to levels similar to pre-industrial times (275–285 ppm), facilitated by deep ocean carbon storage (Seki et al., 2010) and tectonically driven increases in chemical weathering (Raymo and Ruddiman, 1992), was sufficient to induce global cooling and the significant growth of large continental ice sheets (Lunt et al., 2008; Martínez-Botí et al., 2015).

A dramatic increase in IRD abundance during marine isotope stage (MIS) G6 (Flesche Kleiven et al., 2002; Jansen et al., 2000; Jansen and Sjøholm, 1991; Knies et al., 2009; Raymo et al., 1989; Ruddiman and Raymo, 1988) is generally considered to mark the widespread 'intensification' of NHG at ~2.74 Ma. Subsequent IRD pulses recorded at ODP Site 911 on the Yermak Plateau (NW Svalbard) (Knies et al., 2014) (Fig. 2), at ODP Site 909 in the central Fram Strait (Gruetzner et al., 2022), and at ODP Site 986 (W Svalbard) (Butt et al., 2000; Knies et al., 2009) provide further evidence for ice growth on the uplifted Barents Shelf extending well beyond the coastline during the proceeding glacials. A coeval decline of smectite clay minerals both in the Fram Strait and at the western Svalbard margin is thought to reflect a response to the advance of a growing ice sheet to the shelf edge, leading to changes in sediment provenance from distal Siberian shelves (smectite-rich sediments) towards proximal Svalbard–Barents Sea sediment sources (Knies et al., 2009).

For the purposes of constraining our experimental framework, we consider this intensification of NHG as the lower chronological limit for this study. This does not preclude the likelihood that episodes of glacial erosion occurred before this across the Barents Shelf. Indeed, a global cooling event ~3.3 Ma is thought to have triggered an abrupt and severe glaciation during MIS M2 (De Schepper et al., 2009) (Fig. 2). Furthermore, the application of sediment-based proxies may also conceal a more nuanced glacial history, for example, with IRD inputs generally only reflecting the maturing and expansion of continental ice sheets sufficient to impinge on adjacent oceans (Maslin et al., 1998; McClymont et al., 2023).

2.3. Late Plio-Pleistocene uplift and erosion

The current status of Cenozoic (<66 Ma) uplift and erosion on the Norwegian Barents Shelf, which includes its tectonic history, has been comprehensively reviewed by Lasabuda et al. (2021). Despite the large volume of research published, this study identified considerable variations in the magnitude of uplift and erosion proposed between the different methods employed, as well as major uncertainty on the controlling mechanisms responsible. Here, we explicitly examine the role of glaciation and ice sheet erosion in transforming this Arctic region during the most recent 2.74 Ma of the Cenozoic Era – the late Plio-Pleistocene.

Glacial versus pre-glacial sediment volume ratios of 60 %, 50 % and 30 % found in TMFs along the southwestern, northwestern and northern Barents Shelf margins, respectively, demonstrate the profound influence ice sheets had in this region during this lattermost period of the Cenozoic (Lasabuda et al., 2021), with sedimentation rates increasing by an order-of-magnitude at the onset of the late Plio-Pleistocene (Fiedler and Faleide, 1996; Hjelstuen and Sejrup, 2021). Yet, the net impact of glacial processes has been shown to be spatially heterogeneous. In particular, areas of high glacial erosion along the continental margin are largely offset by high glacial deposition of reworked sediments, resulting in low or even no isostatic response of the lithosphere (Zieba et al., 2016). On the contrary, glacial processes across inner parts of the Barents Shelf are considered to account for between a third and two-thirds of all Cenozoic erosion (e.g., Dimakis et al., 1998; Lasabuda et al., 2018b).

Previous attempts to quantify net erosion across the Eurasian Arctic during the Cenozoic have utilised a range of stratigraphic- and physical-based methods. Stratigraphic-based methods typically employ seismic data to quantify eroded intervals/volumes or correlate palaeosurfaces, while physical-based methods rely on a determination and comparison of the physical properties of the bedrock, such as compaction, typically derived from well data. However, estimated net erosion depths across the Barents Shelf derived using these different approaches can vary by up to 1000 m, reflecting the specific uncertainties in these methods (see Lasabuda et al., 2021 for an overview).

One of the most common techniques applied is based on an

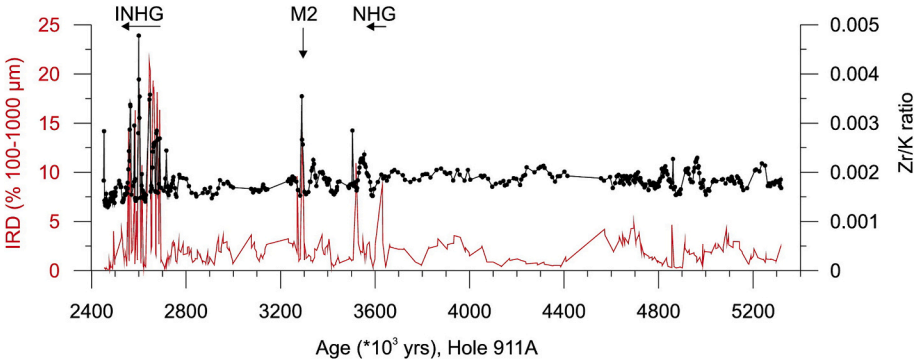

Fig. 2. Ice-rafted debris (IRD) (wt.%) and Zr/K ratio in bulk sediments of ODP Hole 911A, on the Yermak Plateau. The onset of the Northern Hemisphere glaciation (NHG) at ~3.6 Ma sensu Mudelsee and Raymo (2005), the MIS M2 glaciation at ~3.3 Ma, and the intensification of NHG (INHG) at ~2.7 Ma are highlighted. High Zr/K ratios are interpreted as a signature of IRD with a northern Svalbard provenance. Source: Knies et al. (2014).

assumption of mass continuity – an approach in which each stratigraphic layer deposited is assumed to represent the corresponding erosion in the source area. While seismic data coverage and time-depth conversions are critical for accurate estimation of sub-marine sediment volumes, the bulk volume of glacially eroded sediments estimated within the sedimentary wedges along the western and northern Barents Shelf margin has remained relatively consistent across many decades of surveying; recent estimates of 1,334,000 km^3 (Hjelstuen and Sejrup, 2021) and 1,259,000 km^3 (this study) remain within 5 % of original estimates (e.g., Rasmussen and Fjeldskaar, 1996). Yet this mass-balance approach is fundamentally limited by a requirement to precisely define eroded source areas through time, which can be problematic over large glacial catchments such as those on the Barents Shelf. Previous approaches have qualitatively inferred catchment areas based on the present-day landscape (e.g., Laberg et al., 2012; Zieba et al., 2017), or have used a purely geometrical technique to infill eroded concavities, such as fjords, under the assumption that there was an initial paleic surface (Medvedev et al., 2018, 2023).

In this study, we directly tackle these uncertainties by utilizing an empirically constrained ice sheet model to iteratively define glacial catchments backwards through time. The approach exploits our ability to model ice flow across the evolving landscape, and thus optimize the stacking of glacially eroded sediments back onto the shelf according to the modelled patterns of ice discharge. Coupling erosion models with simulations of ice flow and basal thermal dynamics provides a powerful tool for reconstructing ("back-stacking") the spatial detail of landscape development, and is similar to the approach used by Jamieson et al. (2010) to reconstruct the pre-glacial (mid-Cenozoic) landscape evolution of East Antarctica.

2.4. Long-term impacts of glacial erosion of the Barents Shelf

The transformation to an icehouse world during the late Plio-Pleistocene introduced profound changes to glaciated domains during a relatively short period of geologic time. Apart from the significant reshaping of the landscape, the rapid excavation and transport of vast volumes of bedrock directly impacted the Arctic environment far beyond areas touched by glacial ice. To emphasise this, we highlight two examples where long-term glacial erosion and sedimentation have played a significant role through the late Plio-Pleistocene, and where improved landscape models could yield important insights: oceanic circulation and offshore geohazards.

2.4.1. The Barents Seaway

Alongside the Fram Strait and the Bering Strait, the Barents Seaway across the Barents Shelf is one of only three ocean circulation pathways that connect the Arctic Ocean. Today, the Barents Seaway accounts for a net inflow of Atlantic Water of ~1.8 Sv (1 Sv = 1×10^6 m^3 s^{-1}) (Rudels et al., 2015) into the Arctic Ocean, compared to ~6.6 Sv through the Fram Strait (Beszczynska-Möller et al., 2012). As demonstrated by the closure of the Central American Seaway during the late Pliocene, major landscape transformations which block or redirect oceanic circulation can impart major shifts in global climate. For example, recent modelling studies (Hutchinson et al., 2019; Straume et al., 2022) speculate that the closure of Atlantic-Arctic gateways during the Eocene-Oligocene Transition (34 Ma) – either through the Barents Seaway or a proto Fram Strait – acted to initiate Atlantic meridional overturning circulation and drove the climatic cooling that triggered the inception of the Antarctic ice sheet.

The status of the Barents Seaway within palaeoclimate models during the mid-Pliocene (5.3–3.6 Ma) – the last period of Earth's history with higher global temperatures and carbon dioxide levels similar to today (Martínez-Botí et al., 2015) – thus has potentially significant implications. In particular, a subaerial configuration effectively focuses North Atlantic-sourced waters towards the Fram Strait, leading to the concentrated warming of this sector (Butt et al., 2002; Hill, 2015). Similar uplifted and subaerial settings in the Arctic at this time include the Canadian Archipelago and the Great Lakes/Hudson Bay (Dowsett et al., 2016). However, the effects of these topography changes on local and global climate remain poorly understood due to their limited incorporation within general circulation model simulations (Berends et al., 2019).

That the extremely shallow (53 m b.s.l.) Bering Strait, which provides the only alternative connection into the Arctic, was stranded above sea level for the vast majority of the Pleistocene during eustatic lowstands driven by extensive continental glaciation (Farmer et al., 2023), emphasises the critical role of the Barents Seaway in terms of Arctic Ocean inflow. Feedbacks associated with a closed Barents Seaway and increased concentration of Atlantic Waters through the Fram Strait have been cited as a mechanism to explain the apparent discrepancies in the late Cenozoic record of contemporaneous ice-sheet glaciations with 'blue', open-water conditions in the Arctic (Butt et al., 2002). Furthermore, the timing of this bifurcation of Atlantic Waters into the Arctic Ocean potentially explains an increase of extended sea ice and a decrease in primary productivity after 1 Ma, interpreted from proxy data in ODP cores (Stein and Fahl, 2013; Stein and Stax, 1996).

2.4.2. Submarine slope failure

Over-deepened, cross-shelf troughs provide preferential pathways for millions of cubic kilometres of sediment to be transported to the continental slope. The large-scale failure of these slope sediments adjacent to glacially eroded margins is a well-documented phenomenon, with at least 30 such submarine slides reported on the Norway-Barents Sea margin since the onset of NHG (Cherkis et al., 1999; Hjelstuen et al., 2007; Kuvaas and Kristoffersen, 1996; Laberg and Vorren, 1993; Rydningen et al., 2020). Three have occurred within the last 10,000 years (Laberg et al., 2000). The largest of these failure events – referred to as mega-slides – mobilised a sediment volume of up to 25.5×10^3 km^3 down the Bear Island TMF (Hjelstuen et al., 2007). Submarine slope instabilities tend to occur on slopes with remarkably low gradients (<2°) with runout zones spanning hundreds of kilometres (Hampton et al., 1996). Multiple triggers and supporting mechanisms have been proposed to explain these low-angle slope failures, including increased loading through rapid sedimentation, the build-up of excess pore pressure in fine-grained material, glaciomarine and/or contouritic weak layers, seismicity, hydrate dissociation, or asymmetrical ice loading and forebulge development (Baeten et al., 2014; Bellwald et al., 2019b; Hjelstuen et al., 2007; Laberg and Vorren, 2000; Leynaud et al., 2009; Mienert et al., 2005; Pope et al., 2018; Safronova et al., 2017; Winkelmann and Stein, 2007).

Due to their potential to damage seafloor infrastructure and telecommunication cables (Pope et al., 2017), or to generate tsunamis (Harbitz et al., 2006), submarine landslides often pose significant geohazards. That some slopes today exhibit known prerequisites for large sub-marine slide events (Geissler et al., 2016) further highlights the potential risk these major geohazards pose in the Arctic. Refining the timing and pace of the delivery of eroded sediments to the shelf break through the Pleistocene is thus key information to help unravel the evolution of the margin (e.g., Llopart et al., 2015) and distinguish the factors that precondition, and trigger, slope failure.

3. Methods

In the following section we describe how glaciations of the Barents Shelf through the late Plio-Pleistocene are constrained within our modelling framework, the setup of the ice model used to infer patterns of ice discharge during each glacial, how chronostratigraphic data are derived and incorporated to constrain eroded sediment volumes, and how patterns of erosion and isostatic uplift are modelled to iteratively reconstruct the geomorphic evolution of the Barents Shelf topography over each glacial-interglacial cycle. Finally, modelling and methodological limitations are presented.

3.1. Glacial reconstruction

The glacial history of the Eurasian Arctic during the late Plio-Pleistocene is defined here according to the LR04 stack - an average of 57 globally distributed benthic $\delta^{18}O$ records (Lisiecki and Raymo, 2005), using a threshold of 3.7 ‰ to distinguish between glacials and interglacials (e.g., Kleman and Stroeven, 1997) (Fig. 3a). Although this dataset is considered to implicitly represent mean global ice volume, we make the key assumption that it sufficiently captures the evolving intensity and chronology of the glaciations that impacted the Eurasian Arctic over orbital timescales. By setting a minimum glacial duration to 10 ka, 47 individual glacial/interglacial erosion cycles can be defined over the last 2.74 Ma, spanning a total cumulative glacial timeframe of 1.61 Ma.

The extent of glaciation during the late Plio-Pleistocene is considered to have transitioned between various modes, ranging from limited mountain glaciers/ice caps to the more recent continental-scale and longer-lived ice complexes (Hjelstuen and Sejrup, 2021; Kleman et al., 2008; Knies et al., 2009). This transition is reflected by the episodic discharge of massive freshwater pulses captured by long-term climate records from the Arctic, which highlight the dominant and repeating pattern of large ice sheet disintegration and iceberg discharge over the last 0.8 Ma (Flower, 1997; Knies et al., 2007). To broadly capture these shifting modes of glaciation from the LR04 stack through time (Fig. 4a-c), we classify each identified glacial by the associated peak isotope value attained, i.e., mode 1 = ≤4.28 ‰, mode 2 = 4.28–4.54 ‰, and mode 3 = ≥4.54 ‰ (Fig. 3a). This classification thus determines the boundary conditions used by the ice-sheet model to simulate patterns of growth and ice discharge in sync with the evolving shelf topography.

The processing requirements for modelling transient ice sheet dynamics over million-year timescales are not yet feasible, hence a pragmatic and computationally cost-effective alternative is required. We adopt an approach whereby the ice sheet model experiment for each glacial mode was run under a steady climate forcing, with the duration

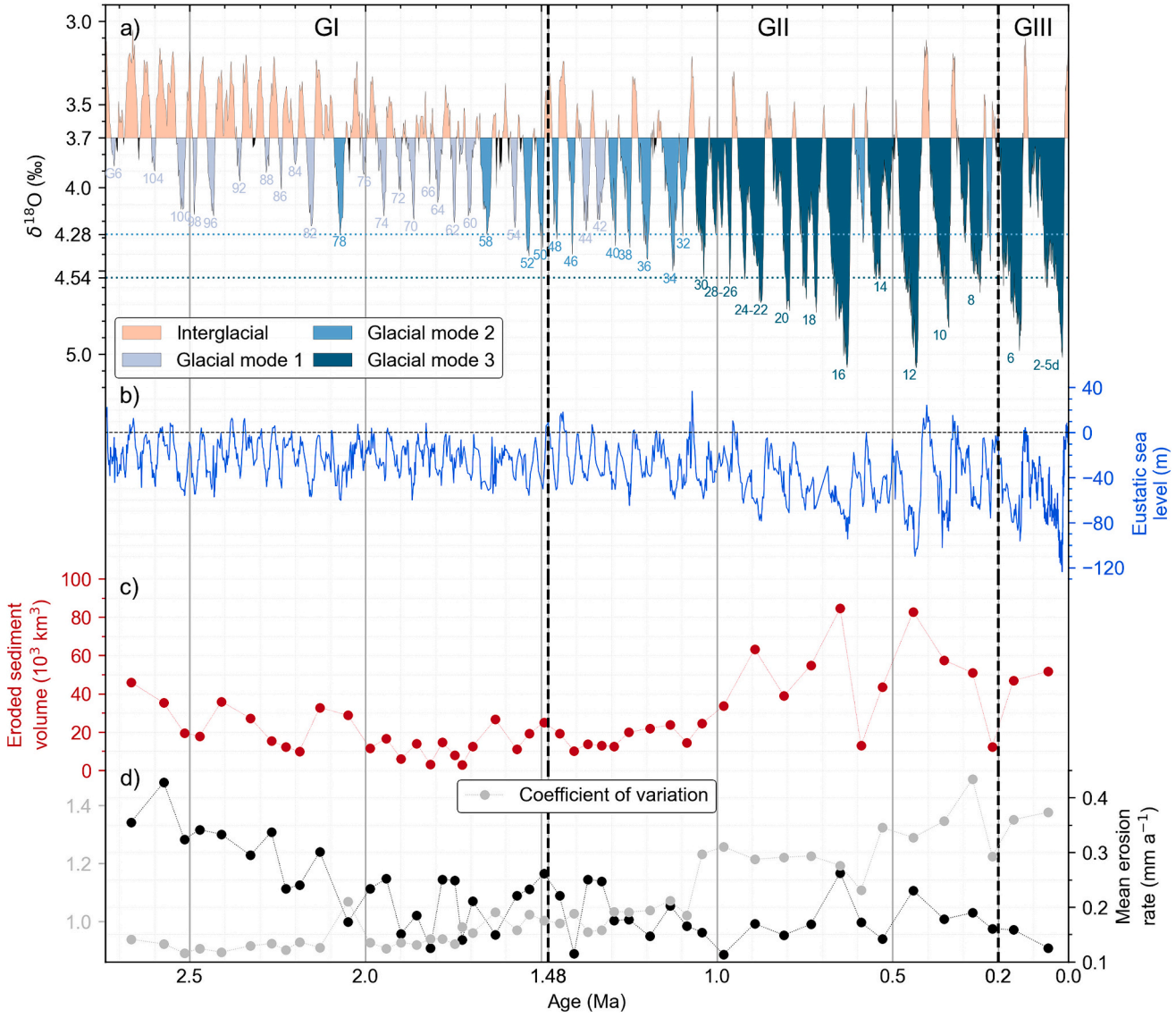

Fig. 3. a) The LR04 $\delta^{18}O$ stack (Lisiecki and Raymo, 2005), partitioned into glacials using a 3.7 ‰ threshold and classified according to the intensity of glaciation (time × deviation) below the $\delta^{18}O$ glacial threshold, and numbered by their respective marine isotope stage. Minor glacials <10 ka (black) are not considered within the erosion model. b) Eustatic sea level, relative to the present day (Miller et al., 2020). c) Calculated eroded sediment volumes that fed the western and northern Barents Sea margin during each glacial of the late Plio-Pleistocene (see Table 3 for respective sources). d) The mean erosion rate (black) from across all glaciated nodes of the modelling domain. The coefficient of variation (grey) is a standardised, unitless measure of dispersion, described by the ratio of the standard deviation to the mean. Intervals defining the major sequences of the off-shelf stratigraphic record (GI-GIII) are based on the framework set out by Alexandropoulou et al. (2021).

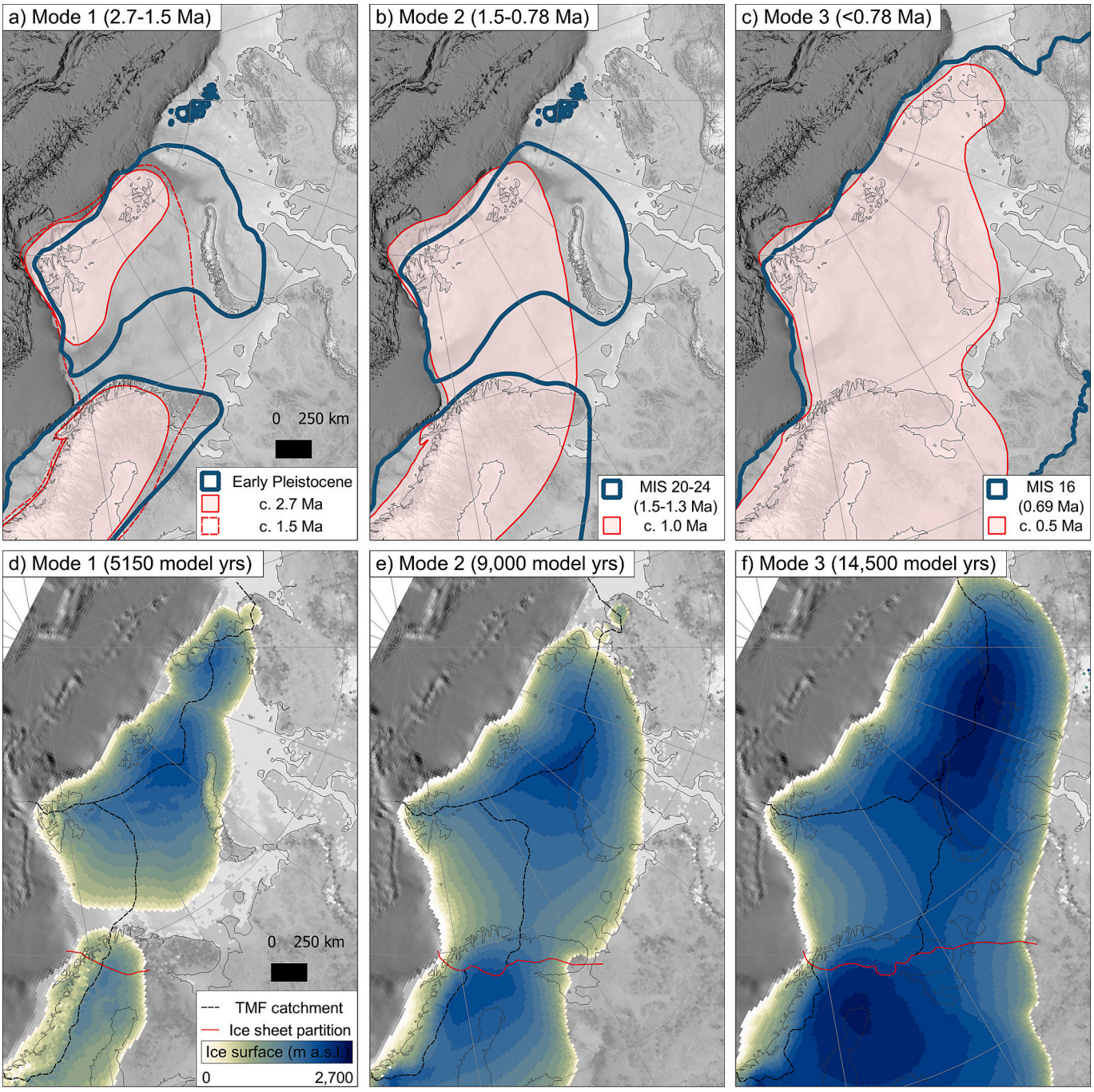

Fig. 4. a-c) Proposed development of the Eurasian ice sheet over northern Fennoscandia and the Barents Shelf through the late Plio-Pleistocene used to constrain the steady-state ice modelling experiments. Red glacial margins are based on sedimentation rates derived from TMFs adjacent to the shelf edge (Hjelstuen and Sejrup, 2021). Blue ice-sheet extents are derived from a synthesis of empirical datasets and numerical modelling studies (Batchelor et al., 2019). Base topography: The GEBCO_2022 Grid. d-f) Examples of modelled peak ice-surface elevation during varying modes of glaciation. The mode, or glacial 'intensity', for each glacial cycle is determined according to the maximum climatic perturbation (Fig. 3a). Mode 1: $\delta^{18}O$ maximum <4.28 ‰; Mode 2: $\delta^{18}O$ maximum 4.28–4.54 ‰; Mode 3: $\delta^{18}O$ maximum >4.54 ‰. TMF catchments (black dashed line) define the source areas for sediments deposited in depocentres off-shelf. The ice-sheet partition (red line) delimits the broader areas where erosion rates derived from the back-stripped TMF catchments are upscaled (see section 3.4, step 2). Both sets of limits are redrawn at each glacial according to the mean ice-discharge configuration. (For interpretation of the references to color in this figure legend, the reader is referred to the web version of this article.)

of the experiment scaled according to the percentage deviation of the peak $\delta^{18}O$ value from the mean of all glacials within that mode. For example, for glacials categorised under mode 3, peak $\delta^{18}O$ values range between 4.54 and 5.08, leading to a model experiment duration ranging from 12,742 to 14,258 model years. This semi-stochastic variability in experiment duration is intended to realistically emulate that of the natural system linked to the transient long-term climate forcing. Although these conceptual model experiments may yield glacial extents dissimilar to those proposed at various timeslices through the Quaternary (cf. Batchelor et al., 2019), a full sensitivity analysis of potential glacial development remains beyond the computational scope of this study.

3.2. The ice model

The numerical ice sheet model used to reconstruct spatial patterns of ice flow dynamics is adapted from Patton et al. (2022) to determine glacial erosion through the last glacial cycle, which is itself based on the model used to reconstruct the glacial evolution of the Eurasian and Icelandic ice sheets through the Last Glacial Maximum (Patton et al., 2016a, 2017a, 2017b). A description of the model and its adaption for the geological timescales required in this study are provided with specific references herein.

Surface mass balance is determined by a positive degree-day scheme, applied according to Laumann and Reeh (1993), and derives total melt from integrated monthly positive temperatures. Despite the limitations of such schemes (Golledge et al., 2010; Seguinot, 2013; van der Veen, 2002), their general ability to simulate glacier responses in contemporary Arctic environments (Braithwaite, 1995; De Woul and Hock, 2005; Jóhannesson et al., 1995) lends confidence in their use. Both temperature and precipitation adjust to the evolving ice sheet surface through applied lapse rates derived from multiple-regression analyses of meteorological observations at a resolution of 1 km from the WorldClim database (Hijmans et al., 2005; version 1.4). To account for the large variations in climate regime across the Eurasian domain, regional reference climates and associated forcing are tuned independently for each of the major ice sheet accumulation centres (from north to south: the Barents Sea, Fennoscandian, and British-Irish ice sheets). An additional mass balance term incorporated is the net water vapour flux to and from the ice sheet surface – a predominant component of ablation in cold continental settings where humidity can be very low (e.g., Frezzotti et al., 2005; Fujii and Kusunoki, 1982).

Calving losses at marine-terminating margins are coupled to relative sea level using a standard empirical function relating the calving flux to ice thickness and water depth (Brown et al., 1982; van der Veen, 2013). The sensitivity of calving to, for example, variations in ocean temperature (Luckman et al., 2015) and sea-ice buttressing (Hoff et al., 2016) has been controlled spatially and temporally through a depth-scaled marine calving/ablation parameterization (Hubbard, 2006). In the absence of explicit calculations of external feedbacks, this depth-related calving coefficient provides a pragmatic and computationally efficient parameterization for determining mass loss at marine-terminating margins of the Eurasian ice sheet. The model is applied to a 20 km finite-difference mesh with the inclusion of grounding-line dynamics based on the analytical boundary treatment of Schoof (Schoof, 2007) and adapted by Pollard and DeConto (2007), which defines the ice flux at the grounding line as a function of ice thickness linearly interpolated between the adjacent node that brackets floating and grounded ice (Hubbard et al., 2009).

Flexure of the lithosphere due to glacier mass directly impacts its architecture, mass balance and flow patterns. Glacial isostatic adjustment is calculated within the ice model using the commonly implemented elastic lithosphere/relaxed asthenosphere (ELRA) scheme, identified by Le Meur and Huybrechts (1996) as a reasonable approach in the absence of a full spherical earth model. A flexural rigidity value of 9.88×10^{24} and a relaxation time of 5000 years were used for each glacial cycle.

3.3. Quantifying eroded bedrock volumes

The chronologically constrained TMF archive provides a valuable proxy for qualifying the spatiotemporal patterns of glacial erosion during the late Plio-Pleistocene, reflecting major shifts in modes of glaciation (Fig. 3a). Eroded sediment volumes used to constrain rates of glacial erosion were derived from these off-shelf depocentres, with three groups used to constrain the pattern and intensity of erosion in and around the Barents Shelf: the northern Barents Sea margin, the western Barents Sea margin, and the mid-Norwegian margin (Fig. 1a).

Sediment depocentres along the Svalbard-Barents Sea margin are characterised by three main seismic units (GI-GIII), within which can be found seven regional seismic reflections (R7-R1) (Faleide et al., 1996). The chronostratigraphy of the Barents Sea margin is thus based on seismic ties of the major sequence boundaries (R7, R5 and R1) to ODP boreholes, with this chronological framework since extended to the Arctic Ocean margin (e.g., Engen et al., 2008; Geissler and Jokat, 2004; Lasabuda et al., 2018a).

The deepest of these units, GI, is interpreted to mark the onset of glacially dominated sedimentation at the Plio-Pleistocene transition ~2.7 Ma (R7) through to 1.5 Ma (R5) (Mattingsdal et al., 2014). However, the onset age for GIII (R1) has historically been assigned varying ages, ranging between <0.7 Ma (Laberg et al., 2010; Lien et al., 2022), 0.44 Ma (Faleide et al., 1996; Sættem et al., 1992) and 0.2 Ma (Butt et al., 2000; Elverhøi et al., 1995; Knies et al., 2009; Rebesco et al., 2014). Here we adopt an age of 0.2 Ma, following the most recent consensus and as proposed by the recent regional and continuous chrono-stratigraphic framework developed by Alexandropoulou et al. (2021).

Further south on the mid-Norwegian margin, late Plio-Pleistocene deposits are found in the Naust Formation (Fig. 1a). This formation is divided into 5 sequences: N (oldest), A, U, S and T (youngest). The chronological framework of this formation is well-established (e.g., Bjordal-Olsen et al., 2023; Dahlgren et al., 2002, 2005; Dowdeswell et al., 2010; Lien et al., 2022; Montelli et al., 2017) with Naust T assumed to be younger than 0.2 Ma (equivalent to R1) and the upper boundary of Naust N assigned an age of 1.5 Ma (equivalent to R5) (Rise et al., 2006).

Sediment volumes at each margin are derived from previously published literature (Table 3), except for the Bear Island TMF for which we present new isopach maps of GI-GIII (Fig. 1b-d). To map the main seismic reflections of R1 (~0.2 Ma), R5 (~1.5 Ma) and R7 (~2.7 Ma) of this TMF we used a dense network of industry- and academia-sourced 2D seismic reflection profiles spanning the last three decades (Fig. 5). This dataset is predominantly focused along the outer continental shelf of the Bear Island Trough and the upper-middle continental slope but is

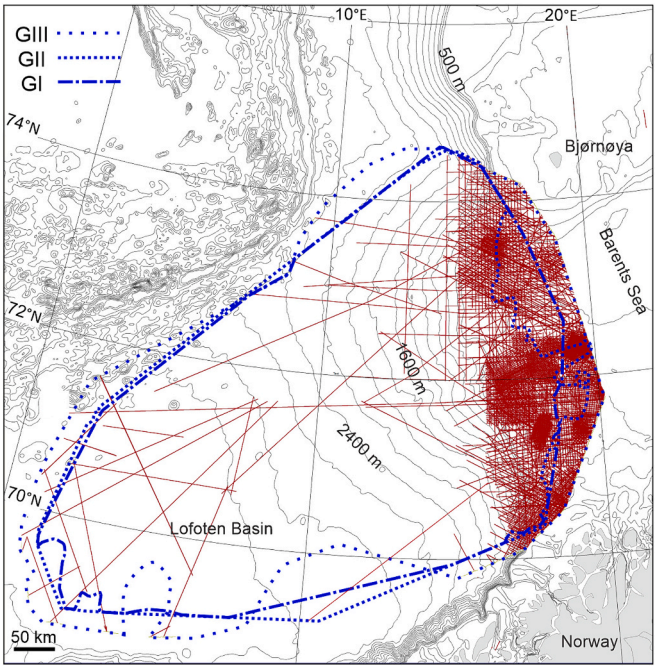

Fig. 5. The network of 2-D seismic profiles (red) used to constrain the sediment volumes within glacial units GIII, GII, and GI (Fig. 1b-d) of the Bear Island trough mouth fan. Contour interval: 200 m. (For interpretation of the references to colour in this figure legend, the reader is referred to the web version of this article.)

supplemented by 20 seismic profiles that cover the entire TMF. The vertical resolution of this dataset (assumed to be 1/4 of the dominant wavelength, λ) varies from 10 to 15 m close to the seafloor and up to 25–30 m near the base of the glacigenic sediments.

Based on the generated seismic horizons, time-thickness maps of the GI-GIII seismic units were produced (Fig. 1b-d). Sediment volumes and average sedimentation rates were calculated for each seismic unit using a time-to-depth conversion based on available velocity constraints (i.e., GI: 2.40 km/s; GII: 2.16 km/s; GIII: 1.97 km/s interval velocity; Fiedler and Faleide, 1996) (Table 1). In all calculations, we assume mass conservation over the depositional area.

With relatively sparse data available from the Arctic Ocean, the total volume estimate by Hjelstuen and Sejrup (2021) of sediments adjacent to the northern Barents Sea margin is subdivided across GI-GIII according to the distribution observed at the Kvitøya TMF (Lasabuda et al., 2018a).

All deposited glacial sediments are corrected with a 5 % compaction factor to provide an erosional volume with a density of 2.2 g cm^{-3}. A further volume reduction is applied when back-stripping sediments over areas of crystalline lithologies to compensate for their generally higher densities of 2.7 g cm^{-3} compared to sedimentary strata. The delimited geological provinces according to Patton et al. (2022) are used to distinguish these contrasting bedrock types.

The eroded volume from each major glacial unit (GI-GIII) is further partitioned for each glacial-interglacial cycle based on the area (time × deviation) of the $\delta^{18}O$ curve above and below 3.7 ‰ (Fig. 3a). As TMFs typically also include deposits from interglacial phases (Vorren and Laberg, 1997), this partitioning of the GI-GIII sediment volumes according to paired glacial and interglacial climate deviations more effectively captures potential subaerial erosion following each deglaciation. This is of particular importance during the late Pliocene and early Pleistocene when the Arctic was dominated by relatively longer interglacials.

3.4. Erosion and uplift modelling

To derive our palaeo-topographic reconstruction of the Eurasian Arctic, cycles of erosion, loading and uplift are iterated for each distinct glacial backwards through time from the present day, redistributing mass and recalculating isostatic equilibrium before the initiation of the previous glacial cycle. Boundary conditions for each glacial-interglacial cycle are summarised in Supplementary Material 2, and the overall iterative framework is as follows:

Step 1: A steady-state ice sheet model is applied on an isostatically relaxed topography, with boundary conditions set to reproduce one of the three modes of glaciation previously inferred for the late Plio-Pleistocene epochs (Fig. 4) (Hjelstuen and Sejrup, 2021; Knies et al., 2009). The mode and duration of each model run are defined according to the maximum climatic perturbation achieved during the glacial based on the LR04 global $\delta^{18}O$ stack (Lisiecki and Raymo, 2005) (Fig. 3a).

Step 2: Catchment areas for the 3 major depocentres (mid-Norwegian, western Barents Sea, and northern Barents Sea margins; Fig. 1) are defined based on the patterns of mean ice discharge predicted by the ice model. With known eroded bedrock volumes (B) for each catchment (Section 3.3; Fig. 3c), an ice sheet erosion parameterization (Patton et al., 2022) is applied to determine the long-term rate of glacial quarrying and abrasion ($\bar{f}$) based on the duration (t_i) and mean rate of ice discharge ($\bar{q}$):

$$\bar{f} = \frac{(B|\sum \bar{q} \times t_i) \times (\bar{q} \times t_i)}{t_i}. \quad (1)$$

Partitioned sediment volumes are hence redistributed across the shelf and terrestrial hinterland based on the mean ice discharge and time glaciated at each cell. For the southeastern catchment that does not directly feed TMF depocentres to the north and west (Fig. 4d-f), the erosion law defined for the western Barents Sea is used to calculate erosion depths. Similarly, erosion across eastern Fennoscandian is scaled based on the erosion law defined for the mid-Norwegian margin. Decompacted glacial-sediment volumes are simultaneously removed across each of the three major depocentres, with the distribution determined by a scaling of the sediment thicknesses mapped in the total Quaternary isopach map (Fig. 1a).

Step 3: Across geological timescales, the redistribution of mass from the continental shelf to the ice sheet margins imparted heterogeneous patterns of tectonic uplift and subsidence within and beyond the formerly glaciated domain, thus forming a significant contribution to net elevation changes. This flexural isostatic adjustment resulting from bedrock erosion and TMF deposition was calculated assuming the lithosphere to represent an elastic plate whose integrated strength is described by an equivalent elastic thickness (EET) (e.g., Burov and Diament, 1995). Here, the open-source model, gFlex (Wickert, 2016), was used to simulate this flexure. Isostatic adjustments were calculated at each interglacial assuming a constant EET of 30 km across the domain. Based on previous studies, this value is considered the most reasonable for this regional study (Amantov and Fjeldskaar, 2018; Medvedev et al., 2023). A clamped boundary condition was used under the assumption of no outside loading. Further input parameter values used can be found in Table 2.

Step 4: The integrated effects of uplift/subsidence and erosion/sedimentation are used to calculate the net topographic change during the particular glacial cycle under scrutiny. The residual at each node is then subtracted from the initial surface to yield a new topographic surface, which is used as the initial input condition to run the next ice sheet model experiment for the preceding glaciation. Given the iterative and incremental nature of this approach to glacial landscape reconstruction and erosion modelling, topographic surfaces at each glacial/interglacial should only be considered first-order approximations.

3.5. Modelling limitations

The Barents Shelf is a relatively data-rich domain with multiple datasets to constrain our study, a result of extensive industry seismic and well data motivated by hydrocarbon exploration. Despite this, there are various factors and underlying assumptions necessary for the application of the ice sheet erosion model, which consequently affects our results and landscape reconstruction. These limitations associated with the methods and constraining datasets and highlighted below are thus potential avenues for further research to improve on these shelf-wide reconstructions.

Table 1
Estimated sedimentation across the Bear Island trough mouth fan (Fig. 1b-d).

Unit	Depositional area (10^3 km^2)	Sediment volume (10^3 km^3)	Avg. sedimentation rate (cm kyr^{-1})
GIII	274	71.4	130.28
GII	244	218.5	69.97
GI	241	86.1	28.72
Combined	274	376.0	55.56

Table 2
Model parameters used to calculate flexural isostasy of the crust associated with glacial erosion and sediment deposition.

Parameter	Value	Units
Young's Modulus	65	GPa
Poisson ratio	0.25	
Effective elastic thickness (EET)	30	km
Mantle density	3300	kg m^{-3}
Seawater density	1030	kg m^{-3}
Sediment (TMF) density	2200	kg m^{-3}
Bedrock density	2700	kg m^{-3}

3.5.1. Eroded sediment volumes

The adjustment of TMF sediment packages through time, based on a scaling of their present-day thickness, neglects to dynamically account for the changing dimensions of the depositional area across the shelf break and TMFs, for example, related to shelf progradation and evolving architecture of the TMF (e.g., Lasabuda et al., 2018a). Furthermore, the approach does not account for the redistribution of these emplaced sediments, for example, along-slope as contourite drifts (e.g., Gebhardt et al., 2014; Rebesco et al., 2013), or down-slope as mega-slides. The largest submarine slide identified so far adjacent to the Barents Shelf is located on the Bear Island TMF, which re-transported $>25.5 \times 10^3$ km^3 of sediments ~1.0–0.78 Ma (Hjelstuen et al., 2007). Further examples have been identified along the north-western Barents Sea margin (cf. Safronova et al., 2017). Altogether, this can lead to thickness discrepancies within individual TMFs at discrete intervals, despite the erosional and sedimentation fluxes remaining in balance over broader spatial and temporal scales.

As the mass-balance technique employed in this study relies on the direct measurement of the deposited sediment volume, the seismic time-depth conversion is a crucial aspect for deriving accurate sediment volume estimates. Time-depth relationships (check-shots) are typically derived from wellbore data. However, wells can be sparsely distributed over large parts of the domain, or even absent in High Arctic areas that are not open for hydrocarbon exploration. The velocity models used in our constraining datasets thus represent an unknown source of error that could modify shelf-wide erosion-rate estimates. In the absence of well data, this uncertainty can be alleviated by acquiring alternative velocity estimates using sonobuoys (equipment deployed along the seismic profile during seismic acquisition) (e.g., Geissler and Jokat, 2004).

3.5.2. Shelf reconstructions

The reworking of older glacial and interglacial sediments during glacial advances, in addition to the volume of sediments not transported to the TMF depocentres, are potential sources of bias in our backstacking calculations. The glacigenic sediment cover found across the Barents Shelf today is variable, ranging from less than a few tens of metres in the central part of the Barents Sea to thicker sequences of up to 300 m that occur near the continental slope and in the southeast (Solheim and Kristoffersen, 1984). For simplicity, we assume the impact of this varying interglacial glacigenic sediment cover naturally attenuates over the multiple cycles of the 2.7 Ma modelling timeframe.

3.5.3. Uplift and ice modelling

The ice-sheet modelling experiments (Fig. 4d-f) are based on a conceptual model for the glaciation of the Barents Shelf during the late Plio-Pleistocene (Hjelstuen and Sejrup, 2021; Knies et al., 2009), which for the most part is based on proxy evidence for glaciation e.g., IRD records, TMF sedimentation rates etc. Knowledge of the extent and intensity of glaciations prior to the last glacial cycle is highly fragmented and, for the most part, unknown (e.g., see Batchelor et al., 2019). The purpose of the ice modelling experiments is thus to provide a glaciologically consistent framework from which the evolving erosional catchments can be tracked over geologic timescales, and are not an explicit reconstruction of glacial dynamics through the late Plio-Pleistocene per se. Investigating and incorporating the potential effects of hemispheric-scale patterns of circulation on ice sheet nucleation, for example, the closing of the Barents Seaway, could hence yield potential new insight into how landscape evolution may have progressed during early phases of the Quaternary when glacial limits are otherwise very poorly constrained.

While the LR04 stack (Fig. 3a) is inherently representative of a global ice volume, we assume this dataset sufficiently captures the evolving intensity and rhythm of glaciation in the Eurasian Arctic over orbital timescales. This does, however, neglect the hemispheric-scale linkages between the Eurasian and North American ice complexes, and the extent these ice masses influenced each other's growth trajectories. For example, the peak glaciation of the Barents-Kara Sea ice sheet during the last glacial cycle was not synchronous with the timing of peak climate deterioration (Svendsen et al., 2004), potentially influenced by the effects of elevated North American paleo-topography on downstream circulation patterns (e.g., Liakka et al., 2016). While we do not explore dynamics within individual glacial cycles, this example highlights the potential disconnect between a global-level proxy for glaciation at the regional scale.

A significant determinant for the magnitude and pattern of isostatic uplift resulting from the mobilization of eroded materials is the implied rigidity of the shelf – the EET. Here, we use a constant EET value, which simplifies the known spatial heterogeneity in the rheological properties of the lithosphere covering Eurasia (Gac et al., 2016; Struijk et al., 2018). From a pragmatic point of view, applying a uniform EET simplifies the erosion modelling procedure by removing the need to recalculate EET changes through the late Plio-Pleistocene. Such an approach, including sensitivity testing of various EET values, is thus an avenue for future investigation.

4. Results

4.1. The glacial impact on the Barents Shelf

Our data-driven modelling analysis demonstrates that a net volume of 1,548,180 km^3 of sediment was excavated and deposited on the continental shelf edge over the 47 individual glaciations spanning the last 2.74 Ma of the late Plio-Pleistocene. This equates to a mean erosion depth of 181 m across the entire glaciated area of the shelf, including a maximum of 2.59 km on the northern Barents Shelf (Fig. 6a). This net volume equates to a ~23 % increase over the sediment volume constrained in the TMF archive (Table 3) since it represents erosion within glacial catchments where ice did not flow towards the continental shelf edge, i.e. to the east and southeast (Fig. 4, Fig. 7).

The scale of this erosion and associated uplift indicates that the pre-glacial topography was primarily subaerial, with the present Barents and Kara seas elevated to a mean position equivalent to present-day sea level at 2.74 Ma (Fig. 8). These hypsometric modifications through the late Plio-Pleistocene were not spatially homogeneous across the shelf though; abundant sedimentation at the shelf break effectively expanded the total area of the continental shelf by ~1 % into the deep ocean (defined by the −600 m contour). Meanwhile, persistent erosion across the northern Barents Shelf denuded potential mountain peaks >500 m above sea level.

Our detailed modelling further reveals the time-transgressive nature of this erosional impact, with the mean erosion rate generally decreasing as the landscape desensitised to successive glaciations, from a peak of 0.43 mm a^{-1} in the early phases of GI to <0.15 mm a^{-1} during the mid-Pleistocene Transition and the most recent, Weichselian, glacial (Fig. 3d). However, this metric alone masks more nuanced insight into the erosive efficacy of ice sheets through the late Plio-Pleistocene. The coefficient of variation – a standardised measure of dispersion that describes the extent of variability in relation to the mean – shows that variations in erosion rates beneath the ice sheet become more dispersed through time, particularly with the onset of more extensive and dynamic shelf-wide glaciations under mode 3 (Fig. 3d). Hence, while large ice sheets during GII and GIII were not as effective overall compared to their more diminutive counterparts during GI, later glaciations were generally characterised by more extreme patterns of erosion ranging from landscape preservation under cold-based ice to more focussed erosion under fast-flowing ice streams.

4.2. Topographic relief evolution

While the modelling experiments were carried out for each glacial-interglacial backwards through time, for simplicity, here we describe the modelled topographic configuration of the Barents Shelf as it evolved through the late Plio-Pleistocene from 2.74 Ma.

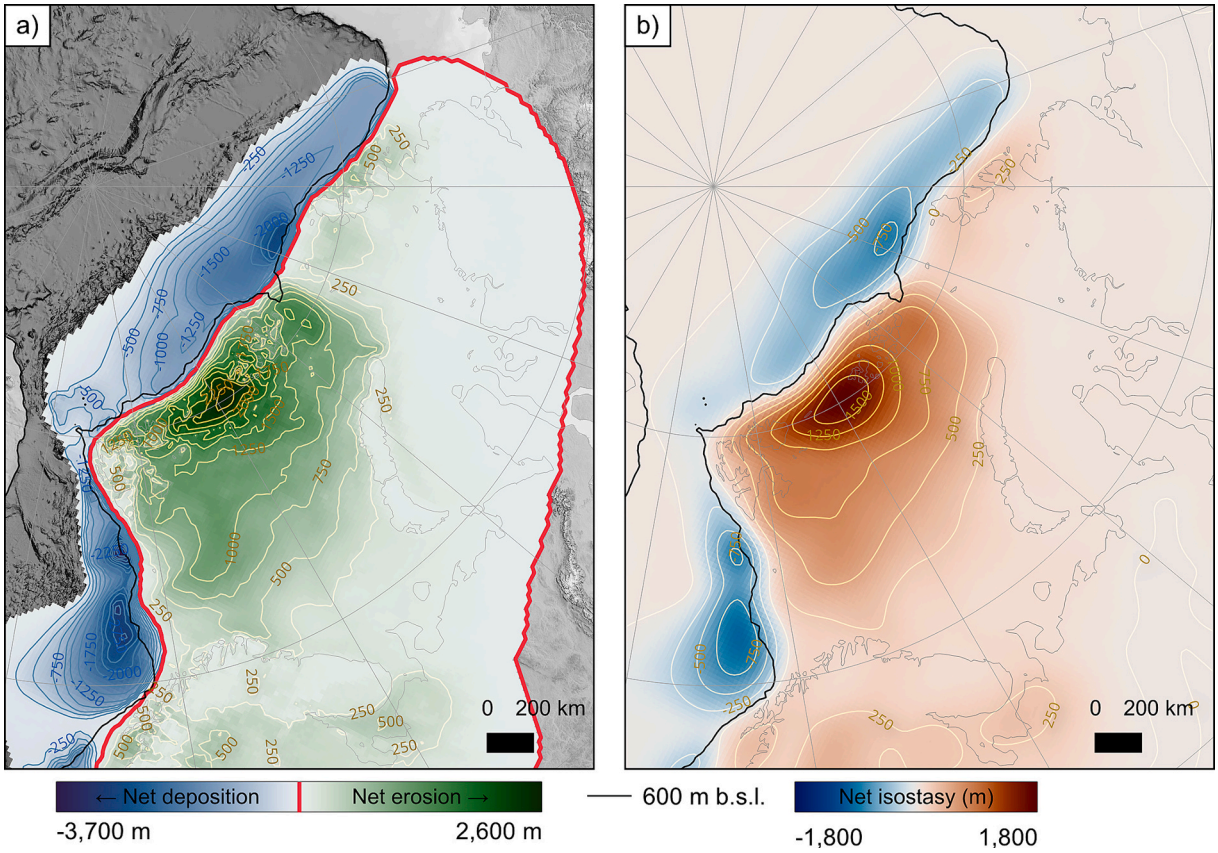

Fig. 6. a) Net deposition and erosion across the Barents Shelf and surrounding regions during the last 2.74 Ma. The red solid line delimits where erosion and deposition are in balance. The 600 m b.s.l. contour marks the approximate location of the present-day shelf break. b) The net total isostatic adjustment of the Barents Shelf and surrounding region in response to glacial erosion and sedimentation spanning the last 2.74 Ma. (For interpretation of the references to colour in this figure legend, the reader is referred to the web version of this article.)

Table 3
Trough mouth fan sediment volumes used to constrain rates and spatial patterns of glacial erosion through the late Plio-Pleistocene. Further details, including average sedimentation rate, can be found in Supplementary Material 1.

	Mid-Norwegian margin	Western Barents Sea				Northern Barents Sea	Barents Shelf combined
	NAUST formation (Dowdeswell et al., 2010)	Bear Island TMF (this study)	Storfjorden TMF (Lien et al., 2022)	West Svalbard (Lien et al., 2022)	Combined	Nansen Basin (Hjelstuen and Sejrup, 2021) †	
GIII (<0.2 Ma)							
Volume (10^3 km^3)	16.30	71.4	7.0	2.00	80.4	18.1	98.5
% of the total volume	15.6	19.0	6.5	6.1	15.6	2.4	7.8
GII (1.48 Ma – 0.2 Ma)							
Volume (10^3 km^3)	54.0	218.5	40.0	10.0	268.5	440.1	708.6
% of the total volume	51.6	58.1	37.4	30.0	52.0	59.2	56.3
GI (2.74 Ma – 1.48 Ma)							
Volume (10^3 km^3)	34.4	86.1	60.0	21.0	167.1	284.8	451.9
% of the total volume	32.9	22.9	56.1	63.6	32.4	38.3	35.9
Total late Plio-Pleistocene (<2.74 Ma)							
Volume (10^3 km^3)	104.7	376.0	107.0	33.0	516.0	743.0	1259.0
% of the Cenozoic volume (10^3 km^3) (ArcCRUST - Petrov et al., 2016)	*N/A*	44.3 (848.3)	45.6 (234.6)	23.1 (143.0)	42.1 (1225.8)	33.3 (2233.1)	36.4 (3459.0)

† Glacial unit (GI - GIII) breakdowns based on chronostratigraphic information from the Kvitøya TMF (Lasabuda et al., 2018a).

4.2.1. GI (2.74–1.48 Ma)

At the late Plio-Pleistocene transition (2.74 Ma) the Barents Shelf is characterised by a subaerial landscape that dominates the present-day northern and central Barents Sea, with the highest terrain (>500 m a.s.l.) extending east from Svalbard towards Franz Josef Land and Novaya Zemlya. Two shallow marine inlets can be found in the locations of the

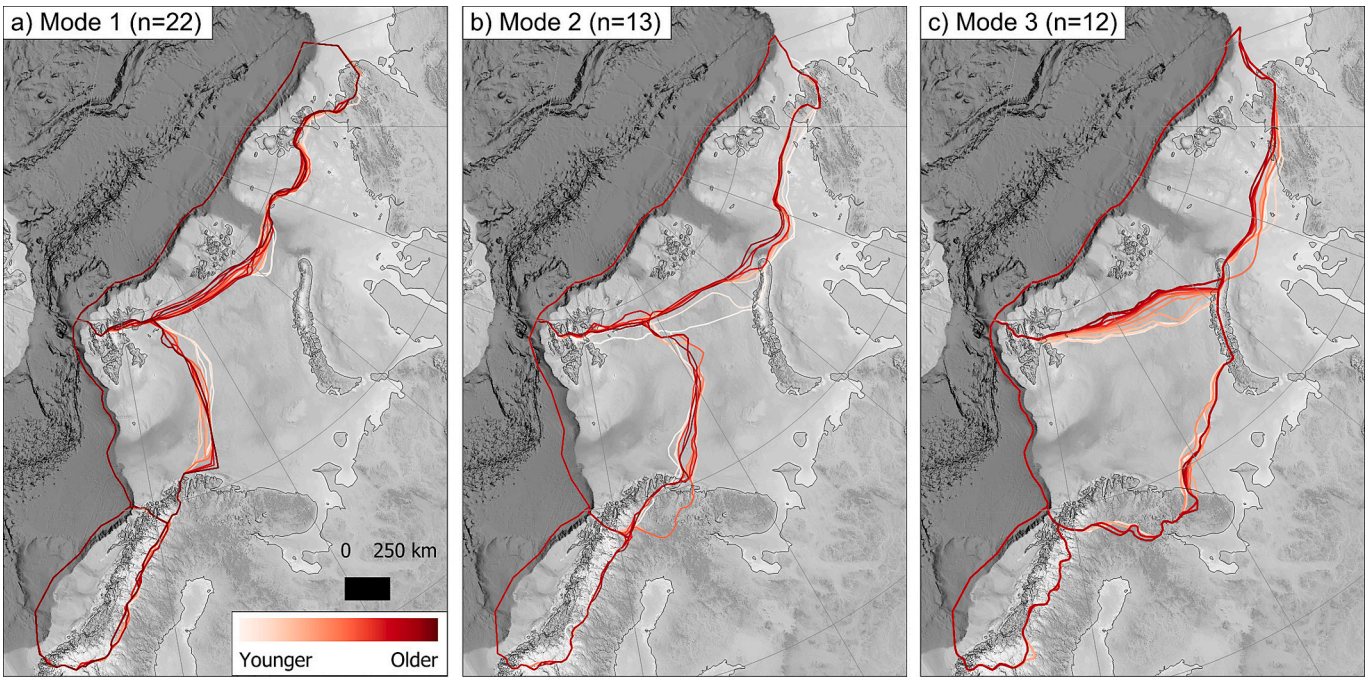

Fig. 7. TMF catchment boundaries and their evolution through time for each glacial during the late Plio-Pleistocene. Base topography: The GEBCO_2022 Grid.

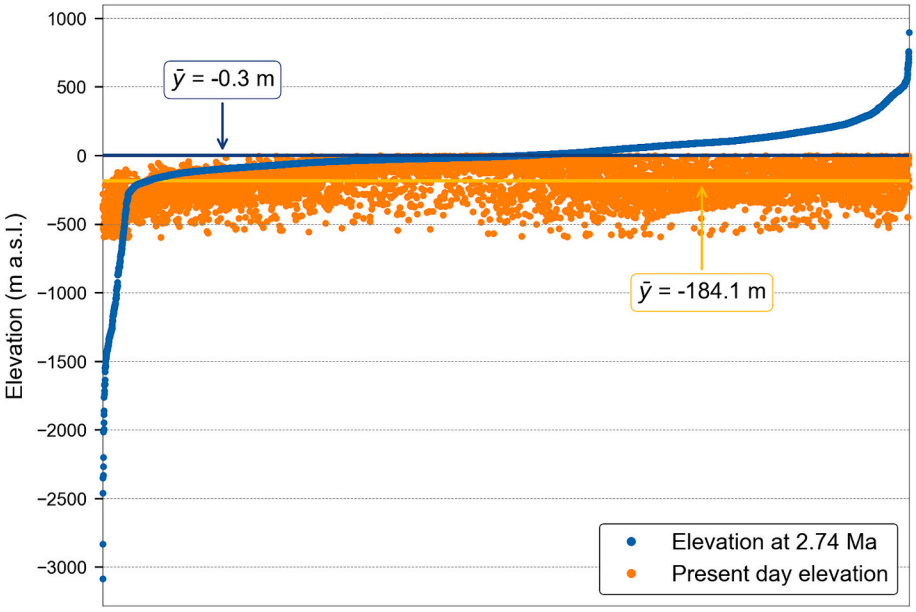

Fig. 8. The evolving hypsometry of the present-day Barents and Kara seas (<0 to >−600 m a.s.l.; mean = −184.1 m a.s.l.) through the late Plio-Pleistocene, directly compared to the respective pre-glacial elevation at 2.74 Ma (blue). Each point from both data series represents a unique grid cell from within the modelling domain. The two series are ordered according to the grid cell's pre-glacial elevation (blue). This pre-glacial domain was, on average, −0.3 m above present-day sea level before the intensification of Northern Hemisphere glaciations, characterised by enhanced terrain over the northern Barents Sea (right), and a retreated position of the entire shelf-edge (left). (For interpretation of the references to colour in this figure legend, the reader is referred to the web version of this article.)

present-day Saint Anna and Bear Island troughs. The southeast Barents Shelf is sub-marine at this time with a water depth of >100 m, though its connection to the Atlantic Ocean by a strait <10 m deep means this basin was likely brackish. The Kara Sea and its coastline are largely recognisable as it is today, albeit with an expanded archipelago of Severnaya Zemlya to the north.

We find that the limited scale of glacial activity (mode 1; Fig. 4a, d) during the late Pliocene and Early Pleistocene has relatively little impact on the broader scale topographic relief. With ice cover largely limited to the northern Barents Shelf and high ground around the present-day archipelagos, these areas experience the greatest topographic lowering. The Saint Anna Trough also widens, though remains less than 200 m deep during GI.

A combination of eustatic variations and isostatic uplift forces brief land bridge connections between Fennoscandia and the rest of the subaerially exposed Barents Shelf throughout GI. From 2.17 Ma, increasing areas of the central Barents Sea become permanently submarine, and by 1.51 Ma the outer Storfjorden Trough has been eroded.

4.2.2. GII (1.48–0.2 Ma)

GII coincides with an uptick in the intensity and duration of glacial cycles across the Northern Hemisphere, and so the Barents Shelf experiences a marked change in the rate of landscape evolution during this interval. It is during this stage that the Barents Shelf transforms from being predominantly subaerial to marine-dominated; by ~1.2 Ma, widespread erosion across central areas leads to this region becoming entirely submerged, characterised by a broad and shallow bank bounded to the east and west by the Central Deep and proto–Bear Island Trough, respectively. The land bridge connecting Svalbard, Franz Josef Land and northern Novaya Zemlya persists though, and is breached for the first time ~0.94 Ma. The final separation of this land bridge is completed after 0.69 Ma.

As well as eroding central areas, the onset of continental-scale glaciations (mode 3; Fig. 4c, f), across the Barents Shelf sees the major ice-streaming pathways continue to deepen, including the outer portions of the Bear Island, Storfjorden and Saint Anna troughs. After 0.7 Ma, the headward expansion of troughs in all sectors accelerates, leading to a shelf configuration at 0.2 Ma that largely resembles the modern-day topography.

4.2.3. GIII (< 0.2 Ma)

The Barents Shelf was overwhelmingly dominated by extensive glaciations during GIII, and saw the continued influence of glacial erosion that also characterised the latter stages of GII. The influence of fast-flowing ice streams associated with repeated shelf-edge glaciations is identifiable through the deepening of troughs along their entire length, most notably in the Storfjorden and Bear Island troughs. Similarly, central and southern bank areas become deeper and narrower with the expansion of minor tributary troughs. The final major change to the Barents Sea configuration occurs during MIS 5e (Eemian; ~115 ka) when the sill damming the White Sea becomes permanently submerged below sea level.

A net result of this excavation of the Barents Shelf over the last 1.48 Ma (GII–GIII) is the advance of the shelf-break position (600 m b.s.l.), by up to 65 km in areas associated with most intense sedimentation, such as the outer troughs of Storfjorden and Bear Island (Fig. 6a).

5. Discussion

5.1. The pre-NHG Barents Shelf configuration

The time-transgressive ice sheet erosion modelling presented reveals that in the last 2.74 Ma, the Eurasian Arctic underwent an extraordinary transition. The landscape shifted from being predominantly subaerial at the end of the Pliocene and characterised by two large embayments straddling an extensive Svalbard / Novaya Zemlya lowland landmass, to a predominantly submerged landscape today. Patterns of net erosion are highly heterogeneous in both space and time, from a maximum of 2.59 km of bedrock removal to <0.1 km. The pattern of net erosion also decreases southward, reaching ~1 km within the Bear Island Trough, reflecting more limited glacial expansion into this sector during the early Pleistocene (Fig. 6a; Fig. 10b). Overall, this regional pattern of erosion is broadly consistent with previous reconstructions of the pre-NHG Barents Shelf, which show large sectors to have been subaerial at the intensification of Northern Hemisphere glaciation (Butt et al., 2002; Dimakis et al., 1998; Lasabuda et al., 2023; Zieba et al., 2017).

In contrast, a recent volumetric mass balance modelling study asserts that the pre-glacial Barents Shelf was mainly submarine, with a mean bathymetry of ~50 to 90 m, or potentially deeper (Medvedev et al., 2023). However, this discrepancy highlights the contrasting methodologies behind the two modelling approaches rather than a reflection of the different datasets incorporated, with two notable differences to consider.

First, the erosional and depositional domains considered in this study are more extensive, accounting for advanced glaciation east of, and over, the present-day Kara Sea that has been well-documented for late Quaternary glacials (Fig. 1; Fig. 4c) (cf. Batchelor et al., 2019). While this substantially increases the sediment volume and extent of deposits considered in the erosion model along this northern Barents Sea margin, this is effectively compensated for by the broader catchments spanning mainland Russia. Despite the volumetric mismatches used between the two studies, the underlying seismic data constraints guiding the glacial sediment reconstructions in this sector are from similar sources (Engen et al., 2009; Jokat and Micksch, 2004; Lasabuda et al., 2018a; Nikishin et al., 2018), and our volumes remain consistent with the qualitatively inferred 30–70 % ratio of glacial-preglacial Cenozoic sediments along this margin (Lasabuda et al., 2021).

Secondly, and importantly, our glaciologically guided approach to catchment reconstruction allows us to constrain the source areas for the off-shelf sediments more effectively through the late Plio-Pleistocene (Fig. 7). This includes identifying glaciated zones that did not directly contribute sediments to the continental slope (namely to the south and east of the domain), and hence why our estimated total erosion of 1,548,180 km^3 from the shelf is greater than the constrained off-shelf sediment volume of 1,259,000 km^3. In contrast, Medvedev et al. (2023) balance off-shelf sediments with eroded material across the entire Barents Shelf.

The nuanced approach presented here which tracks glacial catchment evolution further highlights the probable increased hypsometric variation across the pre-glacial shelf compared to the present day (Fig. 8), with significantly elevated topography across northern sectors, and submarine sectors restricted to the present-day Kara and southeast Barents seas, and the outer Bear Island Trough. However, it should be noted that the Miocene sequence boundary (~20 Ma) was used by Hjelstuen and Sejrup (2021) to constrain our Quaternary isopach volumes in the northern Nansen Basin, in place of no identifiable base late Pliocene boundary in this region. Isopach constraints from this margin should thus be considered an absolute maximum. The northern Barents Shelf configuration modelled here, with elevations exceeding 500 m a.s.l., thus likely represents an end-member solution.

More robust constraints along the western margin, where data coverage is far greater (e.g., Fig. 1, Fig. 5), provide confidence in the accuracy of our modelled shelf evolution across this sector. For example, net erosion estimates at well locations in the outer Bear Island Trough delimit the magnitudes and extent of the transition zone from the dominantly erosive shelf to the mostly depositional outer shelf and continental slope previously modelled by Zieba et al. (2016) (Fig. 11, Table 4). Most of this erosion occurred with the onset of more extensive

Table 4
Late Plio-Pleistocene contributions to net erosion at well locations in the outer Bear Island Trough, as modelled in this study and by Zieba et al. (2016), compared to predicted net erosion through the Cenozoic (Lasabuda et al., 2021).

Well no.	Net erosion (m) (Zieba et al., 2016)			Net erosion (m) (<1.48 Ma; this study)	Cenozoic net erosion (m)
	Min	Mean	Max		
7218/11–1	−294	−139	87	−99 (−34)	681
7219/8–1 S	−161	−5	219	202 (181)	906
7317/10-U-1	−143	13	236	164 (149)	1206
7218/8–1	−138	17	240	152 (139)	732
7219/9–1	−104	51	277	246 (218)	1102
7220/6–1	−83	73	298	386 (346)	1942
7220/8–1	−58	96	322	301 (267)	1393
7220/5–1	−50	101	329	304 (270)	1391

glaciations during GII (<1.48 Ma). While Zieba et al. (2016) were only able to conceptualise the boundary between net erosion and deposition – in effect a pre-NHG shelf break – within the vicinity of these wells in the outer Bear Island Trough, our modelling framework allows us to extend

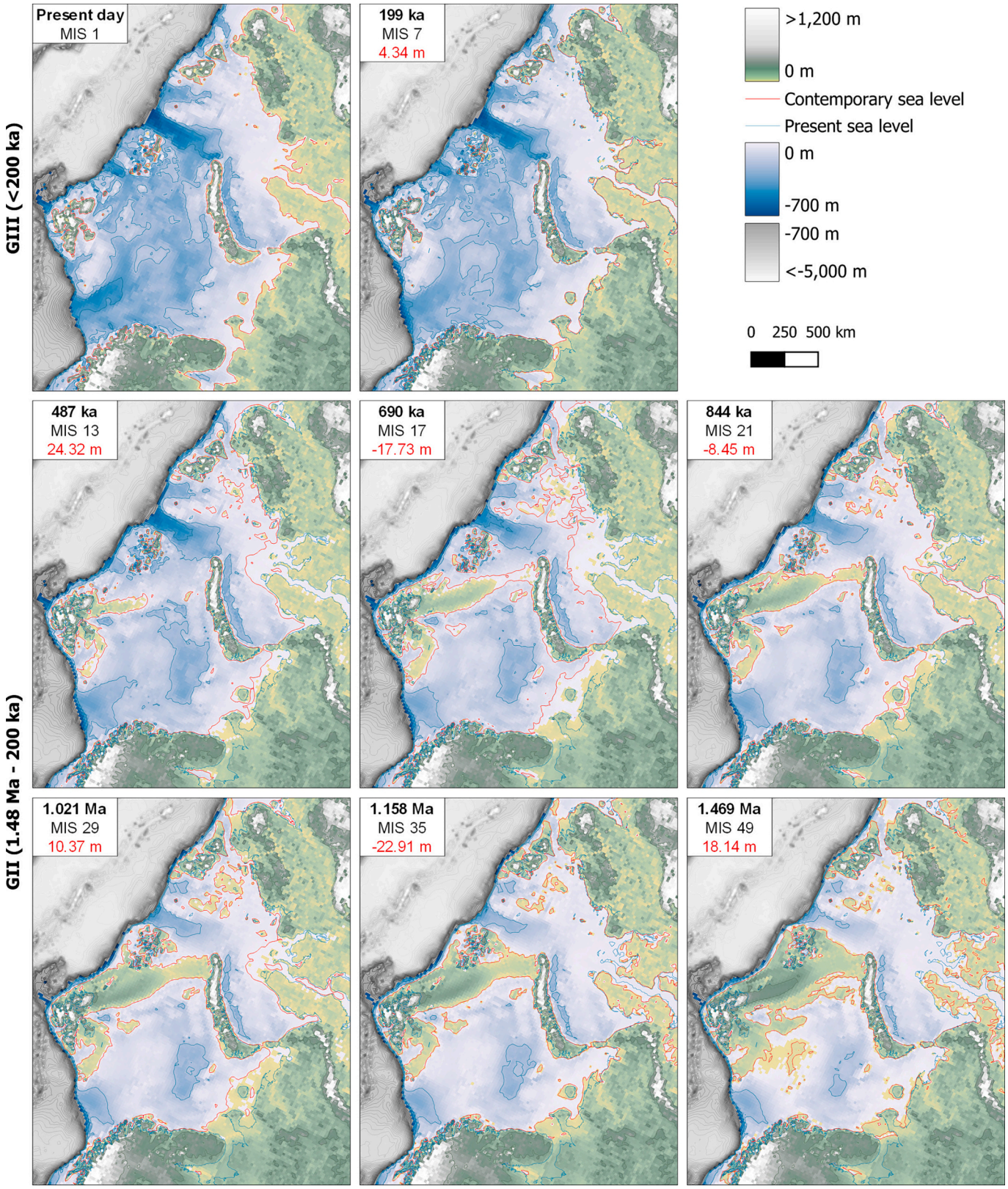

Fig. 9. Evolution of the Barents Shelf during the last 2.74 Ma. All elevations are relative to present-day sea level. Red legend values indicate the contemporary eustatic sea-level position (red line; Fig. 3b). A full timeslice series is provided in Supplementary Material 3. (For interpretation of the references to colour in this figure legend, the reader is referred to the web version of this article.)

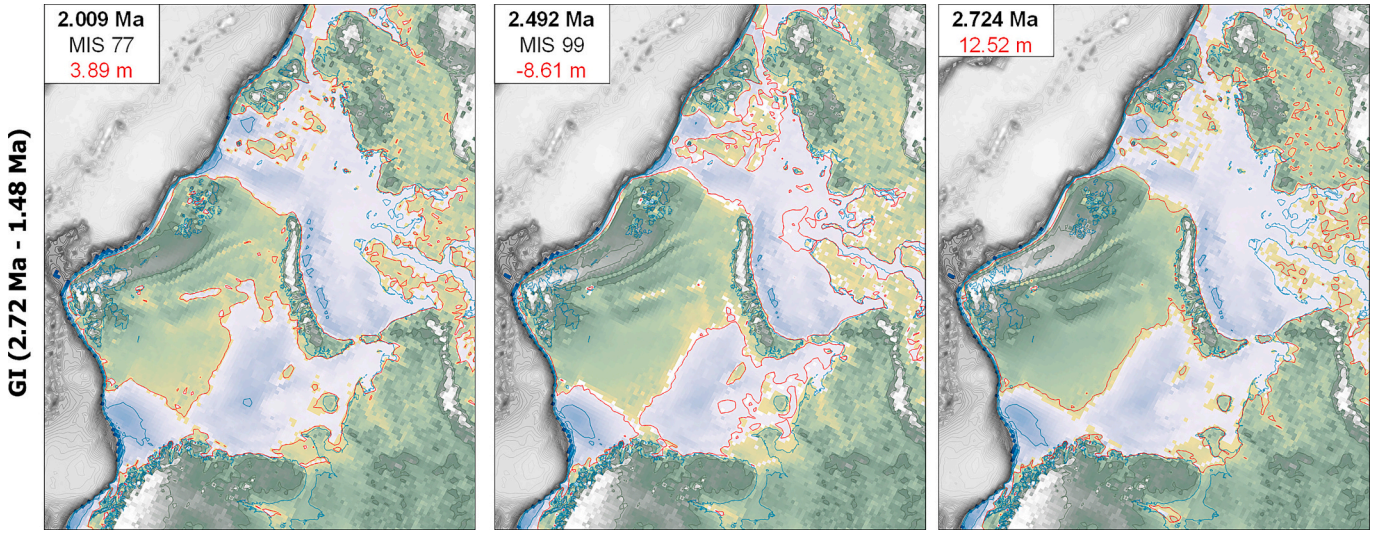

Fig. 9. (*continued*).

this limit to the entire shelf margin (Fig. 6a; Fig. 11).

When modelled net erosion is further compared to the recently synthesised estimates spanning the entire Cenozoic by Lasabuda et al. (2021) it is apparent that the late Plio-Pleistocene glaciations played only a minor role in the net topographic evolution of the outer portions of the western Barents Shelf. In this region where glacial sedimentation largely counters the effects of any glacial erosion, tectonic processes occurring before the Pleistocene tend to dominate the overall uplift along this part of the continental margin (Knies et al., 2014), such as those related to the opening of the Fram Strait (Japsen et al., 2014) or thermal erosion of the mantle lithosphere (Dörr et al., 2013). The importance of tectonic processes over glacial erosion in driving Cenozoic uplift has similarly been argued further south on the Norwegian continental margin (Hall et al., 2013). Elsewhere on the inner parts of the Barents Sea shelf, where sedimentation is largely limited to Last Glacial Maximum deposits (Solheim and Kristoffersen, 1984), processes of glacial erosion thus play a more important role in the overall uplift experienced through the Cenozoic (Lasabuda et al., 2021), and with it, implications for the timing and magnitude of hydrocarbon mobilization and leakage within this petroleum province (e.g., Cavanagh et al., 2006; Kishankov et al., 2022; Serov et al., 2024).

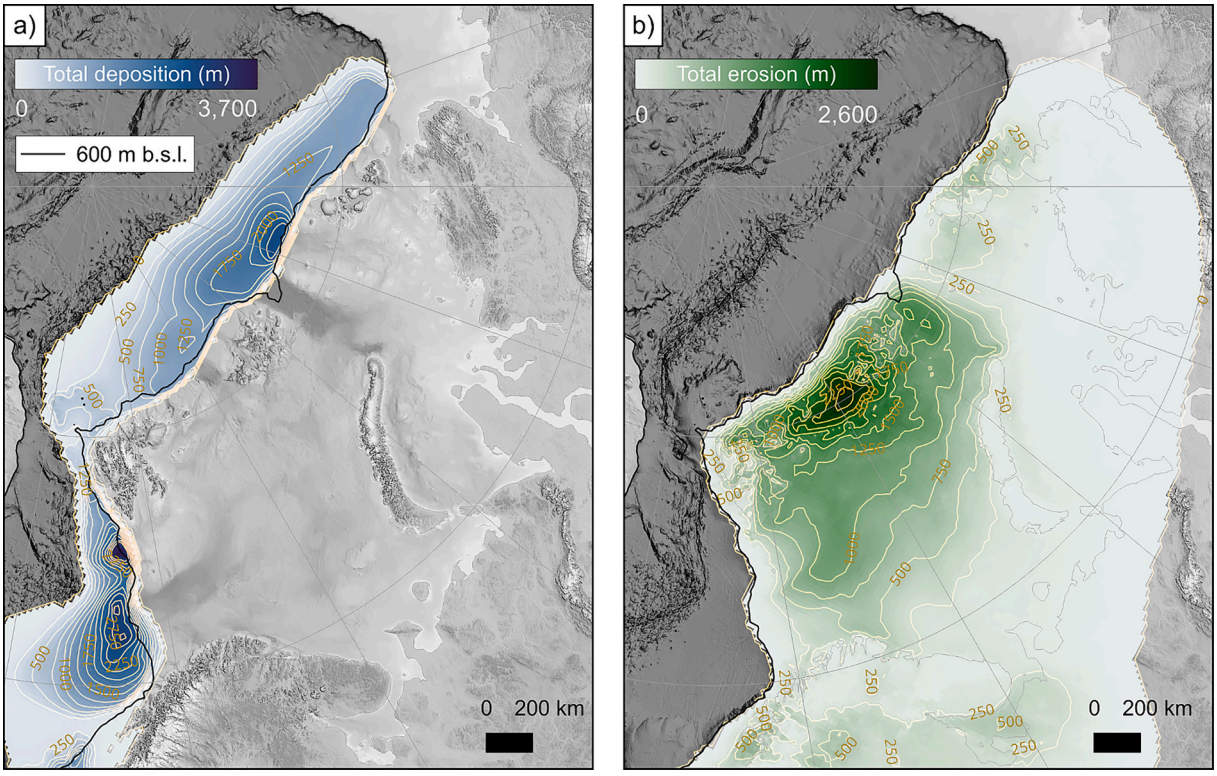

Fig. 10. Total shelf-edge deposition (a) and glacial erosion (b) around the Barents Shelf through the late Plio-Pleistocene. The present-day shelf break is identified by the 600 m b.s.l. contour. Base topography: The GEBCO_2022 Grid.

5.2. Evolution of the modelled Barents Shelf topography

The shaping of the shelf towards its modern-day configuration through the late Plio-Pleistocene can be tracked through the incremental timeslices for each major interglacial (Fig. 9; Supplementary Material 3). Though environmental reconstructions before the intensification of NHG at ~2.74 Ma are poorly constrained, they broadly align with our results here. For example, while seismic data from TMFs along the Arctic (Lasabuda et al., 2018a) and Svalbard (Alexandropoulou et al., 2021; Butt et al., 2000; Hjelstuen et al., 1996) margins contain evidence for shelf-break glaciation during the early Pleistocene, a longstanding interpretation of the palaeoenvironmental constraints in the outer Bear Island Trough reveals ice-free conditions before 1.5 Ma. This interpretation is based on an interpretation of GI paleo-slope sediments as distal glaciomarine, fed by ice that was land-terminating (Laberg et al., 2010) and supported by results from ODP Site 986 (Butt et al., 2000). The identification of mega-scale glacial lineations extending to the palaeo shelf-edge on buried surfaces in this region suggests the southwestern Barents Sea was repeatedly glaciated as early as ~2.6 Ma, potentially from an ice sheet centred over Scandinavia (Harishidayat et al., 2021). The relative proximity of this ice nucleation centre compared to those on the Barents Shelf (Fig. 4d) supports this interpretation of locally sourced ice streaming, though coalescent Barents Sea–Scandinavian ice sheets during this timeframe cannot be completely ruled out.

A switch to more extensive and dynamic ice-sheet coverage with the transition to 100-ka glacial cycles after the mid-Pleistocene Transition (<0.7 Ma) drove intense, selective erosion beneath ice streams. These highly erosive fast-flow features led to the rapid development of glacial troughs that discharged ice west and north to the shelf edge (Fig. 12b). In the largest troughs, such as Bear Island, Saint Anna and Storfjorden, this maturation can be observed by headward glacial deepening towards centres of ice nucleation.

Such highly focussed erosion of major troughs across the shelf also had broader-scale impacts on the net topographic evolution due to enhanced isostatic uplift. This isostatic compensation to glacial erosion drove the isostatic uplift of trough-adjacent bank areas, a process that has been similarly argued to explain the main component of Cenozoic uplift, up to 1.1 km, in central East Greenland (Medvedev et al., 2008). This regional-scale uplift process and the resulting enhancement of topographic relief across adjacent bank areas agrees with previous uplift modelling across the southwest region of the Barents Sea (Zieba et al., 2017).

This net effect is well illustrated by comparing the ratio of uplift to erosion across the entire late Plio-Pleistocene (Fig. 13). Ratio values range from 0, indicating erosion has not been compensated and topography was reduced by erosion alone, to 1 which implies that erosion is entirely compensated by uplift and that the topography has remained stable, or increased when >1. This relationship between erosion and uplift mapped across the Barents Sea demonstrates that enhanced erosion in present-day topographic deeps such as the Bear Island Trough, the coast parallel troughs off northern Fennoscandia, the Central Deep, and Saint Anna Trough has significantly impacted the relative uplift of the central bank area of the Barents Sea and adjacent onshore areas.

This contrasts with the northwestern Barents Shelf where the present-day topographic relief is more subdued. This is primarily a result of an absence of fast-flowing ice streams draining this sector, which would act to selectively focus erosion (Fig. 13). In part, the pattern also reflects the interplay between lithosphere rigidity and the more homogenous distribution of erosion isostatically compensated to a greater magnitude compared to erosion focussed within narrow outlet troughs (Zieba et al., 2017).

The broad and deep erosion patterns across the northern Barents Shelf have remained consistent throughout the late Plio-Pleistocene. Although data constraining the Quaternary isopach along the Arctic Ocean is uncertain (Hjelstuen and Sejrup, 2021; Medvedev et al., 2023),

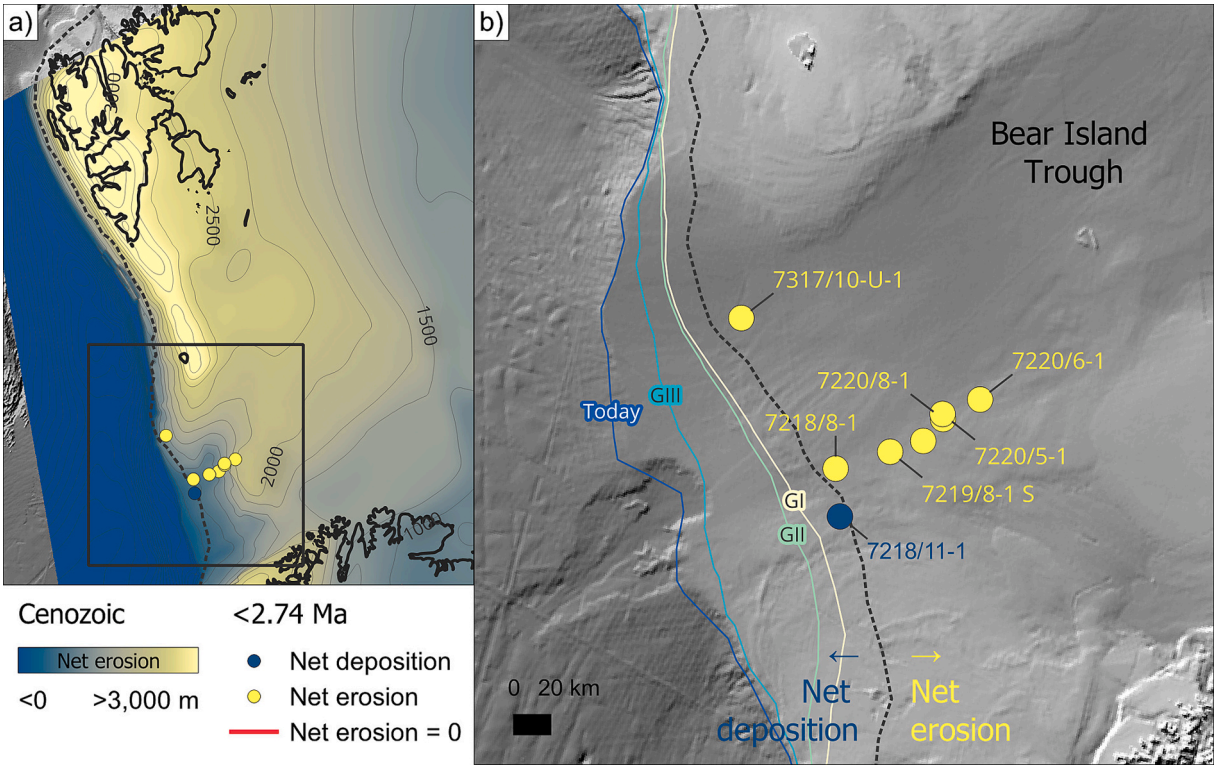

Fig. 11. a) Net Cenozoic erosion map for the greater Barents Shelf (Lasabuda et al., 2021) b) Well locations in the outer Bear Island Trough where net erosion has been previously modelled (Table 4) (Zieba et al., 2016). The dashed line marks the boundary between net erosion and deposition through the late Plio-Pleistocene as modelled in this study (Fig. 6a). Present and palaeo shelf-break positions (600 m b.s.l.) at the base of the three major glacial units are shown with solid lines.

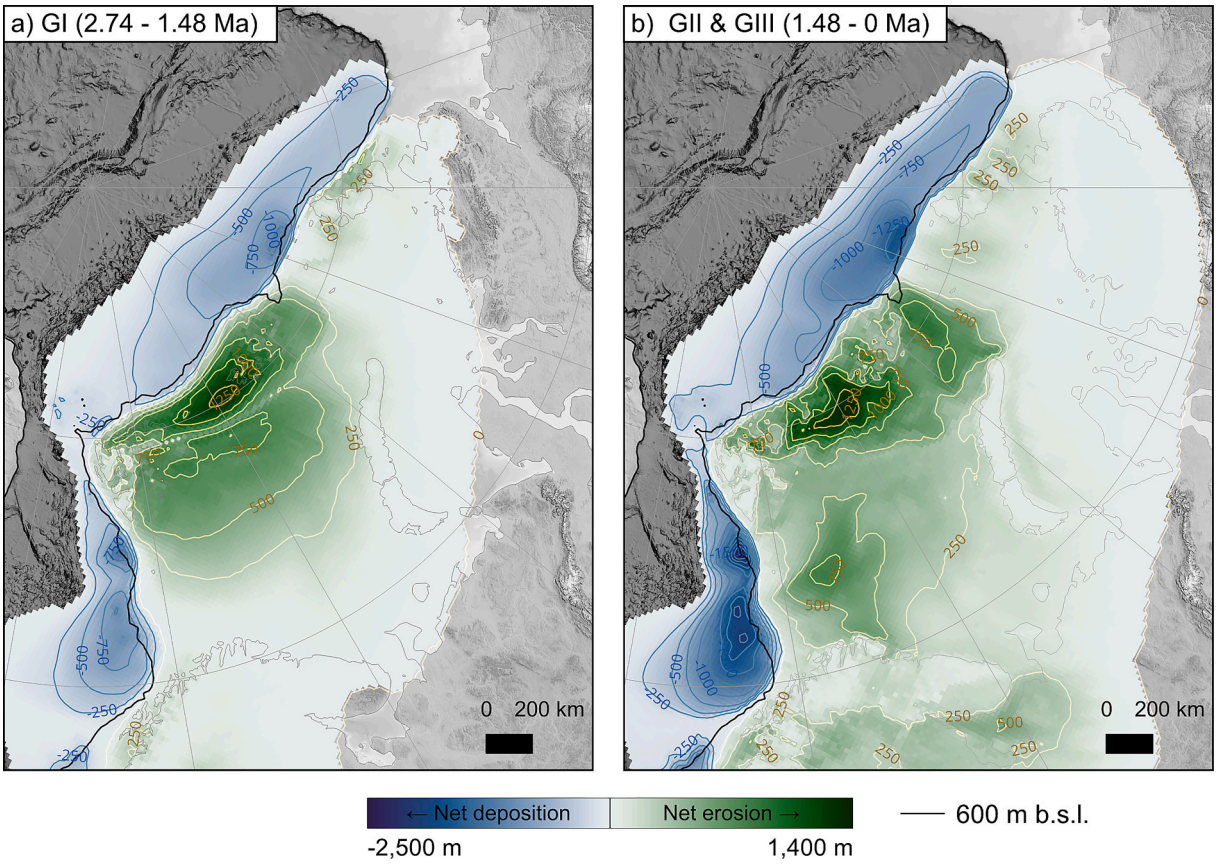

Fig. 12. Net landscape change (erosion/sedimentation) during the late Pliocene to middle Pleistocene (a) and middle Pleistocene to present (b).

it is likely this sector was glacially eroded to a greater extent based on how ice domes and major ice-divides naturally develop during each glacial. On the Barents Shelf, the three high-elevation archipelagos of Svalbard, Franz Josef Land and Novaya Zemlya remain key pinning points for the development of a broad west-east ice divide centred across the northern Barents Sea, even during ice-maximal conditions (Fig. 4d-f). The proximity of these northward-flowing glacial catchments to the shelf break imposes steeper ice-surface gradients, mass-balance gradients, and faster-flowing ice, and hence the potential for considerably more intensive erosion compared to catchments terminating to the south, east or west.

The exception to the deep erosion experienced in this region is the Svalbard archipelago. Constrained by TMF sediment fluxes delivered to the western Barents margin, mountain plateaus are predicted to have experienced relatively modest bedrock lowering, particularly latterly during GII and GIII (32 m versus 101 m during GI; Fig. 12). A similar shift in erosional intensity across this alpine landscape has been observed from cosmogenic nuclide analyses, which show that these summits have largely been preserved for at least the past 1 Ma (Gjermundsen et al., 2015). It is considered this pattern reflects the transition from thin, warm-bedded ice cover to protective armouring under thicker cold-based ice typical of the colder glacial maxima after the mid-Pleistocene Transition.

5.3. *Long-term efficacy of glacial erosion on landscape evolution*

The late Plio-Pleistocene glaciations are closely associated with substantial landscape modification, especially where warm-based, dynamic ice sheets in maritime settings are characterised by fast-flowing ice streams and enhanced subglacial erosion (e.g., Elverhøi et al., 1998; Golledge, 2014). It has been further argued that there is a strong connection between glacial erosion and successive patterns of the ice sheet extent across formerly glaciated regions including North America, Antarctica, Eurasia and Patagonia (e.g., Rabassa and Clapperton, 1990; Singer et al., 2004; Sugden, 1978). Our analysis here presents an ideal natural experiment and an opportunity to quantitatively validate established concepts regarding the long-term efficacy of glacial erosion and landscape development. Particularly, whether a landscape's exposure to prolonged glacial erosion acts to entrench or otherwise destabilize the ice mass (Harbor, 1992; MacGregor et al., 2000; Montgomery et al., 2001; Tomkin and Braun, 2002). In this manner, a glacial 'self-defeating mechanism' has been argued to result in a less extensive ice sheet coverage in successive glaciations over time (MacGregor et al., 2000), and which has been demonstrated for the Scandinavian ice sheet through the Quaternary (Jungdal-Olesen et al., 2024).

The question of the erosive efficacy of ice sheets across the Arctic through the late Plio-Pleistocene has been long debated since early geophysical surveying of TMFs around the Barents Shelf first revealed clues as to their glacial provenance (Eidvin et al., 1993; Elverhøi et al., 1998; Fiedler and Faleide, 1996; Laberg et al., 2012; Lien et al., 2022; Vorren et al., 1989). From the spatially and temporally variable sedimentation rates recorded within these depocentres, it has been recognised that patterns and rates of glacial erosion have varied throughout the late Plio-Pleistocene. For example, based on a study of the Bear Island Trough catchment and TMF in the southwest Barents Sea, Laberg et al. (2012) identified a distinct transition from a state of widespread moderate-to-high erosion during GII to a period of efficient, focused erosion restricted to the troughs during the latest GIII period. Topographic steering was cited as the primary factor driving this partitioning, with a reduced morphological influence on palaeo ice stream locations due to shallower relief during the early to middle Pleistocene (Laberg et al., 2012). Elevated glacial erosion rates of >1.7 mm a^{-1} inferred beneath the Vestfjord ice stream (mid Norway) (Laberg et al., 2009) and >4 mm a^{-1} beneath the Bear Island ice stream during the last glacial

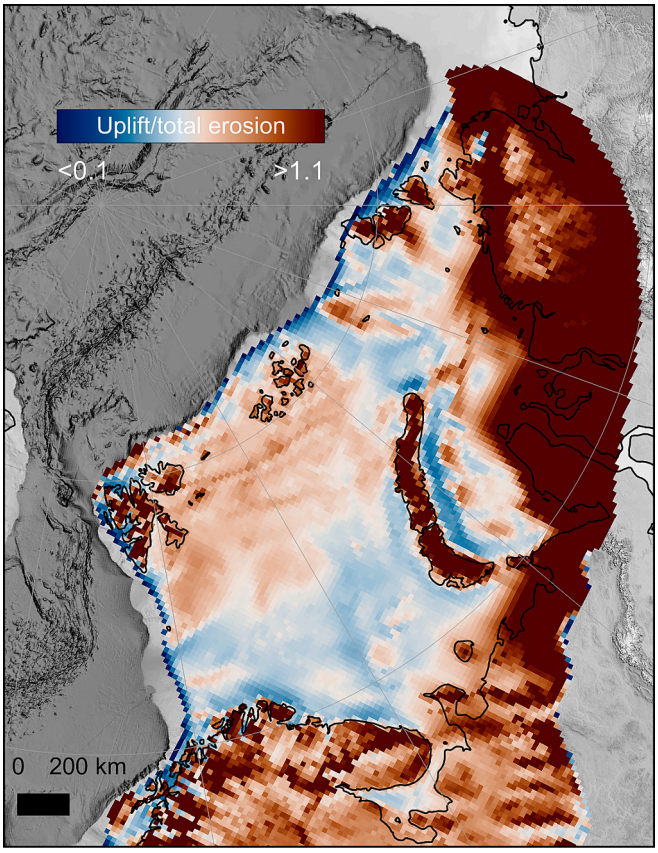

Fig. 13. Uplift to total erosion ratio in areas of net uplift (Fig. 6b). Potential ratio values range from 0, indicating erosion has not been compensated and topography was reduced by erosion alone, to ≥1 which implies that erosion is entirely compensated by uplift and that the topography has remained stable or increased.

cycle (Patton et al., 2022) demonstrate the potential effectiveness of focussed ice flow within this Arctic setting.

The development of the first continuous seismostratigraphic framework for the 1000-km long Svalbard-Barents Sea margin over the last 2.7 Ma (Alexandropoulou et al., 2021) has since allowed more detailed insight into glacial dynamics across the region. The sedimentation record presents a series of glacial intensification and expansion at 1.95 Ma and 1.5 Ma. Yet, as the ice masses expanded during GII, sedimentation rates subsequently decreased between ~1.2 and 0.78 Ma, indicating a diminishing erosional capacity and/or gradual reduction in the availability of readily erodible unlithified material. The widespread erosion of preglacial regolith has been cited as a potential regulator of ice-sheet dynamics and the transition from 41,000 to 100,000-year glacial cycles (Clark and Pollard, 1998; Willeit et al., 2019). It thus follows that large sectors of the Barents Shelf were subaerially exposed and weathered before NHG intensification.

Further phases of increased sedimentation rates at ~0.78 Ma and 0.42 Ma on the southwest Barents Shelf margin are tied to increasing topographic control on ice streaming and the expansion of glacial catchment areas, respectively, linked to more pronounced glacial expansion eastwards beyond the Kara Sea (Alexandropoulou et al., 2021). Meanwhile, sedimentation rates west of Svalbard have remained relatively consistent over the last 1.2 Ma.

However, this chronostratigraphic framework and model for glacial erosion across the Barents Shelf has since been challenged by Lien et al. (2022), who present an almost contrary timeline of landscape development since the mid-Pleistocene Transition. From 1.5 Ma to 0.8 Ma, Lien et al. (2022) found sedimentation rates almost tripled compared to the early Pleistocene, thought to reflect the development of a prominent ice stream in the Bear Island Trough (Harishidayat et al., 2021). Following 0.8 Ma, a dramatic reduction in glacial sediment input took place along the western margin of the Barents Shelf, indicating the erosional capacity of the BSIS reduced by more than 75 %. Meanwhile, sediment inputs on the mid-Norwegian margin doubled, and increased fivefold for the North Sea TMF. Despite no apparent reduction in ice-streaming activity in the Bear Island Trough (Andreassen et al., 2007; Bellwald et al., 2019a; Waage et al., 2018), Lien et al. (2022) suggested various factors to explain the erosional drop-off, including the submergence of the Barents Shelf during this period, the reduced availability of regolith to erode, and a shift to more widespread cold-based conditions across topographic banks and highs.

That such contrasting potential scenarios exist for the long-term landscape evolution of the Barents Shelf reflects not just the difficulty of inferring insights from low-temporal resolution stratigraphic records, but also the inconsistent stratigraphic chronologies used, particularly the age of the R1 regional seismic reflector that defines the boundary between the major glacial units of GII and GIII. Alexandropoulou et al. (2021) have previously summarised the historical uncertainties surrounding the age determination for this sequence boundary. As in this study, they assigned an age of 0.2 Ma for R1 within their stratigraphic framework, based on its position between seismic reflections at the ODP Site 986 that correspond to ~0.13 Ma and 0.42 Ma (west of Svalbard) (Knies et al., 2009) and other recently published chronologies (Dessandier et al., 2021; Rebesco et al., 2014). Lien et al. (2022) favoured a more conservative estimate of 0.7 Ma, in line with previous assessments of the unreliability of amino acid analyses (e.g., Laberg et al., 2010) that had favoured a younger age of <0.44 Ma (Sættem et al., 1992).

Despite the contrasting chronologies of up to 0.5 Ma for R1, a consistent theme apparent from this modelling and previous literature (Alexandropoulou et al., 2021; Laberg et al., 2012) is that the development of ice stream catchments during shelf-wide glaciations was a major factor driving the increasing effectiveness of glacial erosion and sediment evacuation across the Barents Shelf over the last 1 Ma. However, feedbacks associated with topographic entrenchment during the late Pleistocene – whereby focussed erosion eventually limits the potential for subsequent ice cover to erode the landscape (e.g., Jungdal-Olesen et al., 2024; Patton et al., 2016b) are not identified and probably reflect the relatively immature glacial overdeepening of the shallow-relief Barents Shelf as visible today (Fig. 13). Indeed, ice streaming through the inner Bear Island Trough during the Last Glacial Maximum was effectively decoupled from the underlying topography during ice-maximum conditions (Piasecka et al., 2016), indicating that topographic steering was only relevant during periods of thinning ice cover, such as deglaciation.

5.4. *The opening of the Barents Seaway*

Palaeobathymetric reconstructions of the southwest Barents Sea by Lasabuda et al. (2023) suggest that the Barents Seaway remained closed throughout most of the Cenozoic (<55 Ma), with the Fram Strait remaining the only Arctic gateway since its opening in the Miocene ~17 Ma (Engen et al., 2008; Jakobsson et al., 2007). Under intense levels of glacial erosion during the Quaternary, the Barents Seaway was glacially excavated and reopened sometime between 1 and 0.7 Ma (Butt et al., 2002; Zieba et al., 2017). Our modelling analysis here confirms this assessment and that the new pathway for low-to-high latitude circulation was intermittently open as early as 0.94 Ma (MIS 25), and permanently in place after ~0.69 Ma (MIS 17) (Fig. 9).

Initial development of the Barents Seaway can be tracked from GI when a shallow (<100 m) marine environment across the southern Barents Shelf becomes permanently established at <2 Ma (MIS 49). This shallow marine zone continues to widen and deepen throughout GII, allowing Atlantic Water to penetrate across the inner shelf eastwards towards Novaya Zemlya. A fully open connection through to the

northeast Barents Sea and the Arctic Ocean occurs ~0.69 Ma with the dissection of the land bridge connecting the current archipelagos of Novaya Zemlya and Franz Josef Land. Selective ice-sheet erosion associated with the most recent extensive glaciations, including the Elsterian (MIS 12, 478 ka), Late Saalian (MIS 6, ~200 ka) and Weichselian (MIS 5d – 2, ~115 ka) played a critical role in the deepening of this Barents Seaway, enhancing the topographic relief of the major glacial troughs that dissect the northern and western shelf (Fig. 9).

6. Conclusions

Recently compiled, and newly revised, trough-mouth fan sediment volumes from around the Eurasian Arctic are used to constrain detailed spatial and temporal patterns of glacial erosion, sedimentation, and uplift across the Barents and Kara seas during each distinct glacial spanning the last 2.74 Ma. A thermomechanical model of ice sheet dynamics and an elastic lithospheric plate model are applied iteratively to reconstruct the detailed topographic surfaces at high resolution for each of the 47 interglacials through the late Plio-Pleistocene since the intensification of Northern Hemisphere glaciation. Key insights into the landscape evolution of the Eurasian Arctic can be summarised as follows:

- A compilation of industry- and academic-sourced data is used to revise Bear Island trough-mouth fan isopach volumes for each major package, GI-GIII. Increased resolution across this sediment depocentre yields a revised total late Plio-Pleistocene volume of 376 × 10^3 km^3, around 12 % lower than previous estimates (e.g., Lien et al., 2022).
- Exploiting an improved chronology, we adopt the chronostratigraphic framework of Alexandropoulou et al. (2021) to constrain the distinct phases of glacial development and sedimentation observed across the Barents Shelf margins (GI: ~2.7–1.5 Ma; GII: 1.5–0.2 Ma; GIII: <0.2 Ma).
- We determine that erosion of the Barents Shelf and its terrestrial hinterland equated to 1,548,180 km^3 over the entire 47 glacial-interglacial cycles spanning the late Plio-Pleistocene. This represents a 23 % increase over the 1,259,000 km^3 volume constrained within off-shelf trough mouth fan depocentres - a residual difference due to our modelling of erosion within glacial catchments that did not directly feed the continental margin.
- The scale of this net erosion and associated uplift meant that at the intensification of Northern Hemisphere glaciation at ~2.74 Ma, large expanses of the Eurasian Arctic were subaerially exposed. Shallow marine environments existed though in the outer Bear Island Trough, as well as in the southeast Barents and Kara seas. The switch from a largely subaerial to a submarine landscape across the present-day central Barents Sea occurred between 2.0 and 1.5 Ma.
- A maximum of 2.59 km of bedrock was eroded along the northern margin of the Barents Shelf between Svalbard and Franz Josef Land during the late Plio-Pleistocene, in areas proximal to ice-sheet nucleation. Across the southern Barents Sea, the impact of glacial erosion was less severe, with over 1 km of bedrock eroded within the Bear Island Trough. Most of the denudation of the southern Barents Sea occurred within the last 1.5 Ma when the ice sheet, drained by fast-flowing streams regularly advanced southwards, and coalesced with the Fennoscandian ice sheet.
- The opening of the Barents Seaway, which created a second connection between the Atlantic and Arctic oceans, developed after ~0.94 Ma (MIS 25) following the erosion of the land bridge connecting northern Novaya Zemlya to the archipelagos of Franz Josef Land and Svalbard. The seaway has remained fully open since ~0.69 Ma (MIS 17). This connection through the High Arctic proceeded a widening of the shallow marine zone across the southern Barents Shelf after ~2 Ma.
- The development of the bathymetric relief of the Barents Shelf as recognisable today, including the central bank areas and large cross-shelf troughs that discharged glacial ice north and west from the shelf interior, accelerated during the most recent shelf-wide glaciations <1 Ma.
- Mean erosion rates show a general decrease through time, from a peak of 0.43 mm a^{-1} in the early phases of GI to <0.15 mm a^{-1} during the mid-Pleistocene Transition and the most recent, Weichselian, glacial. However, the variation in erosion rates becomes more dispersed over time, with more extensive and dynamic shelf-wide glaciations exhibiting more extreme patterns of erosion.
- The switch to more intense, selective erosion beneath large, fast-flowing ice streams increased the efficacy of erosion within glacial troughs, which in turn drove enhanced isostatic uplift of trough-adjacent bank areas across the southern Barents Sea.
- Delimiting the volumes and chronology of glacially eroded sediments along the northern Barents Sea margin, particularly in the northern Nansen Basin, remains a primary obstacle for accurately constraining landscape evolution using current mass-balance approaches.

CRediT authorship contribution statement

Henry Patton: Conceptualization, Methodology, Formal analysis, Investigation, Software, Visualization, Writing – original draft, Writing – review & editing. **Nikolitsa Alexandropoulou:** Conceptualization, Formal analysis, Visualization, Writing – review & editing. **Amando P. E. Lasabuda:** Conceptualization, Writing – review & editing. **Jochen Knies:** Conceptualization, Writing – review & editing. **Karin Andreassen:** Conceptualization, Funding acquisition, Project administration, Writing – review & editing. **Monica Winsborrow:** Conceptualization, Writing – review & editing. **Jan Sverre Laberg:** Conceptualization, Writing – review & editing. **Alun Hubbard:** Conceptualization, Funding acquisition, Methodology, Writing – original draft, Writing – review & editing.

Declaration of competing interest

The authors declare that they have no known competing financial interests or personal relationships that could have appeared to influence the work reported in this paper.

Data availability

Palaeo-topography digital elevation models of the Eurasian Arctic from each interglacial through the Quaternary are available from https://doi.org/10.18710/3DNZCM.

Information about the availability of the 2D seismic profiles acquired by UiT is available by contacting the corresponding author.

Acknowledgements

This research is a part of iC3: Centre for ice, Cryosphere, Carbon and Climate, the Centre for Arctic Gas Hydrate Environment and Climate (CAGE), and The Centre for Planetary Habitability (PHAB), and was supported by the Research Council of Norway (RCN) through its Centres of Excellence funding scheme, project no. 223259, 332635 and 332523, and the *Akademia* Programme at Equinor.

Amando P. E. Lasabuda acknowledges funding from the European Union's Horizon Europe research and innovation programme under the Marie Skłodowska-Curie Actions (grant no. 101102324), and the Research Council of Norway (grant no. 349791).

In addition to RCN funding, Alun Hubbard gratefully acknowledges an Arctic Five Chair (UiT), a research fellowship from the University of Oulu funded by Arctic Interactions (ArcI- Academy of Finland PROFI4 grant no. 318930), the FARIA network, and the Research Council of

Finland (grant no. 363970).

Norwegian Offshore Directorate is acknowledged for providing 2D seismic data through the Diskos National Data Repository (NDR). The seismic data are available for academic purposes through NDR (http://www.diskos.no/).

We thank TGS ASA for permission to access and reproduce 2D seismic data from the southwestern Barents Sea.

Schlumberger is acknowledged for the Petrel software under an educational license agreement to the Department of Geosciences, UiT The Arctic University of Norway.

Appendix A. Supplementary data

TMF breakdown.csv – Trough mouth fan volume constraints used in the modelling, including the depositional area and average sedimentation rate (expanded from Table 3). Boundary conditions.csv – A detailed breakdown of the boundary condition data used in the erosion modelling at each glacial. Timeslices.zip – Palaeo-topography figures for each of the 47 interglacial timeslices through the Quaternary (expanded from Fig. 9). Supplementary data to this article can be found online at https://doi.org/10.1016/j.earscirev.2024.104936.

References

Alexandropoulou, N., Winsborrow, M., Andreassen, K., Plaza-Faverola, A., Dessandier, P.-A., Mattingsdal, R., Baeten, N., Knies, J., 2021. A Continuous Seismostratigraphic Framework for the Western Svalbard-Barents Sea margin over the last 2.7 Ma: Implications for the late Cenozoic Glacial history of the Svalbard-Barents Sea Ice Sheet. Front. Earth Sci. 9. https://doi.org/10.3389/feart.2021.656732.

Amantov, A., Fjeldskaar, W., 2018. Meso-Cenozoic exhumation and relevant isostatic process: the Barents and Kara shelves. J. Geodyn. 118, 118–139. https://doi.org/10.1016/J.JOG.2017.12.001.

Andreassen, K., Odegaard, C.M., Rafaelsen, B., 2007. Imprints of former ice streams, imaged and interpreted using industry three-dimensional seismic data from the South-Western Barents Sea. Geol. Soc. Lond. Spec. Publ. 277, 151–169. https://doi.org/10.1144/GSL.SP.2007.277.01.09.

Baeten, N.J., Laberg, J.S., Vanneste, M., Forsberg, C.F., Kvalstad, T.J., Forwick, M., Vorren, T.O., Haflidason, H., 2014. Origin of shallow submarine mass movements and their glide planes—Sedimentological and geotechnical analyses from the continental slope off northern Norway. J. Geophys. Res. Earth 119, 2335–2360. https://doi.org/10.1002/2013JF003068.

Bartoli, G., Sarnthein, M., Weinelt, M., Erlenkeuser, H., Garbe-Schönberg, D., Lea, D.W., 2005. Final closure of Panama and the onset of northern hemisphere glaciation. Earth Planet. Sci. Lett. 237, 33–44. https://doi.org/10.1016/j.epsl.2005.06.020.

Batchelor, C.L., Margold, M., Krapp, M., Murton, D.K., Dalton, A.S., Gibbard, P.L., Stokes, C.R., Murton, J.B., Manica, A., 2019. The configuration of Northern Hemisphere ice sheets through the Quaternary. Nat. Commun. 10, 1–10. https://doi.org/10.1038/s41467-019-11601-2.

Bellwald, B., Planke, S., Lebedeva-Ivanova, N., Piasecka, E.D., Andreassen, K., 2019a. High-resolution landform assemblage along a buried glacio-erosive surface in the SW Barents Sea revealed by P-Cable 3D seismic data. Geomorphology 332, 33–50. https://doi.org/10.1016/j.geomorph.2019.01.019.

Bellwald, B., Urlaub, M., Hjelstuen, B.O., Sejrup, H.P., Sørensen, M.B., Forsberg, C.F., Vanneste, M., 2019b. NE Atlantic continental slope stability from a numerical modeling perspective. Quat. Sci. Rev. 203, 248–265. https://doi.org/10.1016/j.quascirev.2018.11.019.

Berends, C.J., de Boer, B., Dolan, A.M., Hill, D.J., van de Wal, R.S.W., 2019. Modelling ice sheet evolution and atmospheric CO_2 during the late Pliocene. Clim. Past 15, 1603–1619. https://doi.org/10.5194/cp-15-1603-2019.

Beszczynska-Möller, A., Fahrbach, E., Schauer, U., Hansen, E., 2012. Variability in Atlantic water temperature and transport at the entrance to the Arctic Ocean, 1997–2010. ICES J. Mar. Sci. 69, 852–863. https://doi.org/10.1093/icesjms/fss056.

Bjordal-Olsen, S., Rydningen, T.A., Laberg, J.S., Lasabuda, A.P.E., Knutsen, S.-M., 2023. Contrasting Neogene–Quaternary continental margin evolution offshore mid-north Norway: Implications for source-to-sink systems. Mar. Geol. 456, 106974. https://doi.org/10.1016/j.margeo.2022.106974.

Braithwaite, R.J., 1995. Positive degree-day factors for ablation on the Greenland ice sheet studied by energy-balance modelling. J. Glaciol. 41, 153–160. https://doi.org/10.3198/1995JoG41-137-153-160.

Brown, C.S., Meier, M.F., Post, A., 1982. Calving Speed of Alaska Tidewater Glaciers, with Application to Columbia Glacier (No. 1258– C). Professional Paper. U.S. Geological Survey.

Burov, E.B., Diament, M., 1995. The effective elastic thickness (T_e) of continental lithosphere: what does it really mean? J. Geophys. Res. Solid Earth 100, 3905–3927. https://doi.org/10.1029/94JB02770.

Butt, F.A., Elverhøi, A., Solheim, A., Forsberg, C.F., 2000. Deciphering late Cenozoic development of the western Svalbard Margin from ODP Site 986 results. Mar. Geol. 169, 373–390. https://doi.org/10.1016/S0025-3227(00)00088-8.

Butt, F.A., Drange, H., Elverhøi, A., Otterå, O.H., Solheim, A., 2002. Modelling late Cenozoic isostatic elevation changes in the Barents Sea and their implications for oceanic and climatic regimes: preliminary results. Quat. Sci. Rev. 21, 1643–1660. https://doi.org/10.1016/S0277-3791(02)00018-5.

Cavanagh, A.J., Di Primio, R., Scheck-Wenderoth, M., Horsfield, B., 2006. Severity and timing of Cenozoic exhumation in the southwestern Barents Sea. J. Geol. Soc. Lond. 163, 761–774. https://doi.org/10.1144/0016-76492005-146.

Cherkis, N.Z., Max, M.D., Vogt, P.R., Crane, K., Midthassel, A., Sundvor, E., 1999. Large-scale mass wasting on the North Spitsbergen continental margin, Arctic Ocean. Geo-Mar. Lett. 19, 131–142. https://doi.org/10.1007/s003670050100.

Clark, P.U., Pollard, D., 1998. Origin of the Middle Pleistocene transition by ice sheet erosion of regolith. Paleoceanography 13, 1–9. https://doi.org/10.1029/97PA02660.

Clark, P.U., Shakun, J.D., Rosenthal, Y., Köhler, P., Bartlein, P.J., 2024. Global and regional temperature change over the past 4.5 million years. Science 383, 884–890. https://doi.org/10.1126/science.adi1908.

Cohen, K.M., Finney, S.C., Gibbard, P.L., Fan, J.-X., 2013. The ICS International Chronostratigraphic Chart. Episodes J. Int. Geosci. 36, 199–204. https://doi.org/10.18814/epiiugs/2013/v36i3/002.

Dahlgren, K.I.T., Vorren, T.O., Laberg, J.S., 2002. Late Quaternary glacial development of the mid-Norwegian margin—65 to 68°N. Mar. Pet. Geol. 19, 1089–1113. https://doi.org/10.1016/S0264-8172(03)00004-7.

Dahlgren, K.I.T., Vorren, T.O., Stoker, M.S., Nielsen, T., Nygård, A., Sejrup, H.P., 2005. Late Cenozoic prograding wedges on the NW European continental margin: their formation and relationship to tectonics and climate. Mar. Pet. Geol. 22, 1089–1110. https://doi.org/10.1016/j.marpetgeo.2004.12.008.

De Schepper, S., Head, M.J., Groeneveld, J., 2009. North Atlantic current variability through marine isotope stage M2 (circa 3.3 Ma) during the mid-Pliocene. Paleoceanography 24. https://doi.org/10.1029/2008PA001725.

De Schepper, S., Schreck, M., Beck, K.M., Matthiessen, J., Fahl, K., Mangerud, G., 2015. Early Pliocene onset of modern Nordic Seas circulation related to ocean gateway changes. Nat. Commun. 6, 8659. https://doi.org/10.1038/ncomms9659.

De Woul, M., Hock, R., 2005. Static mass-balance sensitivity of Arctic glaciers and ice caps using a degree-day approach. Ann. Glaciol. 42, 217–224. https://doi.org/10.3189/172756405781813096.

Dessandier, P.-A., Knies, J., Plaza-Faverola, A., Labrousse, C., Renoult, M., Panieri, G., 2021. Ice-sheet melt drove methane emissions in the Arctic during the last two interglacials. Geology 49, 799–803. https://doi.org/10.1130/G48580.1.

Dimakis, P., Braathen, B.I., Faleide, J.I., Elverhøi, A., Gudlaugsson, S.T., 1998. Cenozoic erosion and the preglacial uplift of the Svalbard–Barents Sea region. Tectonophysics 300, 311–327. https://doi.org/10.1016/S0040-1951(98)00245-5.

Dörr, N., Clift, P.D., Lisker, F., Spiegel, C., 2013. Why is Svalbard an island? Evidence for two-stage uplift, magmatic underplating, and mantle thermal anomalies. Tectonics 32, 473–486. https://doi.org/10.1002/tect.20039.

Dowdeswell, J.A., Ottesen, D., Rise, L., 2010. Rates of sediment delivery from the Fennoscandian Ice Sheet through an ice age. Geology 38, 3–6. https://doi.org/10.1130/G25523.1.

Dowsett, H., Dolan, A., Rowley, D., Moucha, R., Forte, A.M., Mitrovica, J.X., Pound, M., Salzmann, U., Robinson, M., Chandler, M., Foley, K., Haywood, A., 2016. The PRISM4 (mid-Piacenzian) paleoenvironmental reconstruction. Clim. Past 12, 1519–1538. https://doi.org/10.5194/cp-12-1519-2016.

Eidvin, T., Jansen, E., Riis, F., 1993. Chronology of Tertiary fan deposits off the western Barents Sea: Implications for the uplift and erosion history of the Barents Shelf. Mar. Geol. 112, 109–131. https://doi.org/10.1016/0025-3227(93)90164-Q.

Elverhøi, A., Svendsen, J.I., Solheim, A., Andersen, E.S., Milliman, J., Mangerud, J., Hooke, R.LeB, 1995. Late Quaternary Sediment Yield from the High Arctic Svalbard Area. J. Geol. 103, 1–17. https://doi.org/10.1086/629718.

Elverhøi, A., Hooke, R.LeB, Solheim, A., 1998. Late Cenozoic erosion and sediment yield from the Svalbard-Barents Sea region: implications for understanding erosion of glacierized basins. Quat. Sci. Rev. 17, 209–241. https://doi.org/10.1016/S0277-3791(97)00070-X.

Engen, Ø., Faleide, J.I., Dyreng, T.K., 2008. Opening of the Fram Strait gateway: a review of plate tectonic constraints. Tectonophysics 450, 51–69. https://doi.org/10.1016/j.tecto.2008.01.002.

Engen, Ø., Gjengedal, J.A., Faleide, J.I., Kristoffersen, Y., Eldholm, O., 2009. Seismic stratigraphy and sediment thickness of the Nansen Basin, Arctic Ocean. Geophys. J. Int. 176, 805–821. https://doi.org/10.1111/j.1365-246X.2008.04028.x.

Faleide, J.I., Solheim, A., Fiedler, A., Hjelstuen, B.O., Andersen, E.S., Vanneste, K., 1996. Late Cenozoic evolution of the western Barents Sea-Svalbard continental margin. Glob. Planet. Chang. 12, 53–74. https://doi.org/10.1016/0921-8181(95)00012-7.

Faleide, J.I., Abdelmalak, M.M., Minakov, A., Meza-Cala, J.C., Lasabuda, A.P.E., Gaina, C., Drachev, S.S., 2024. Eurasia Basin Composite Tectono-Sedimentary Element, 57. Geological Society, London. https://doi.org/10.1144/M57-2023-16. M57-2023–16. Memoirs.

Farmer, J.R., Pico, T., Underwood, O.M., Cleveland Stout, R., Granger, J., Cronin, T.M., Fripiat, F., Martínez-García, A., Haug, G.H., Sigman, D.M., 2023. The Bering Strait was flooded 10,000 years before the last Glacial Maximum. Proc. Natl. Acad. Sci. 120, e2206742119. https://doi.org/10.1073/pnas.2206742119.

Fiedler, A., Faleide, J.I., 1996. Cenozoic sedimentation along the southwestern Barents Sea margin in relation to uplift and erosion of the shelf. Glob. Planet. Chang. 12, 75–93. https://doi.org/10.1016/0921-8181(95)00013-5.

Flesche Kleiven, H., Jansen, E., Fronval, T., Smith, T.M., 2002. Intensification of Northern Hemisphere glaciations in the circum Atlantic region (3.5–2.4 Ma) – ice-rafted detritus evidence. Palaeogeogr. Palaeoclimatol. Palaeoecol. 184, 213–223. https://doi.org/10.1016/S0031-0182(01)00407-2.

Flower, B.P., 1997. Overconsolidated section on the Yermak Plateau, Arctic Ocean: Ice sheet grounding prior to ca. 660 ka? Geology 25, 147–150. https://doi.org/10.1130/0091-7613(1997)025.
Frezzotti, M., Pourchet, M., Flora, O., Gandolfi, S., Gay, M., Urbini, S., Vincent, C., Becagli, S., Gragnani, R., Proposito, M., Severi, M., Traversi, R., Udisti, R., Fily, M., 2005. Spatial and temporal variability of snow accumulation in East Antarctica from traverse data. J. Glaciol. 51, 113–124. https://doi.org/10.3189/172756505781829502.
Fujii, Y., Kusunoki, K., 1982. The role of sublimation and condensation in the formation of ice sheet surface at Mizuho Station, Antarctica. J. Geophys. Res. Oceans 87, 4293–4300. https://doi.org/10.1029/JC087iC06p04293.
Gac, S., Klitzke, P., Minakov, A., Faleide, J.I., Scheck-Wenderoth, M., 2016. Lithospheric strength and elastic thickness of the Barents Sea and Kara Sea region. Tectonophys. SI Circum-Arctic Evol. 691, 120–132. https://doi.org/10.1016/j.tecto.2016.04.028.
Gales, J., Hillenbrand, C.-D., Larter, R., Laberg, J.S., Melles, M., Benetti, S., Passchier, S., 2019. Processes influencing differences in Arctic and Antarctic trough mouth fan sedimentology. Geol. Soc. Lond. Spec. Publ. 475, 203–221. https://doi.org/10.1144/SP475.7.
Gebhardt, A.C., Geissler, W.H., Matthiessen, J., Jokat, W., 2014. Changes in current patterns in the Fram Strait at the Pliocene/Pleistocene boundary. Q. Sci. Rev. 92, 179–189. https://doi.org/10.1016/j.quascirev.2013.07.015.
Geissler, W.H., Jokat, W., 2004. A geophysical study of the northern Svalbard continental margin. Geophys. J. Int. 158, 50–66. https://doi.org/10.1111/j.1365-246X.2004.02315.x.
Geissler, W.H., Gebhardt, A.C., Gross, F., Wollenburg, J., Jensen, L., Schmidt-Aursch, M. C., Krastel, S., Elger, J., Osti, G., 2016. Arctic megaslide at presumed rest. Sci. Rep. 6, 38529. https://doi.org/10.1038/srep38529.
Gjermundsen, E.F., Briner, J.P., Akçar, N., Foros, J., Kubik, P.W., Salvigsen, O., Hormes, A., 2015. Minimal erosion of Arctic alpine topography during late Quaternary glaciation. Nat. Geosci. 8, 789–792. https://doi.org/10.1038/ngeo2524.
Golledge, N.R., 2014. Selective erosion beneath the Antarctic Peninsula Ice Sheet during LGM retreat. Antarct. Sci. 26, 698–707. https://doi.org/10.1017/S0954102014000340.
Golledge, N., Hubbard, A., Bradwell, T., 2010. Influence of seasonality on glacier mass balance, and implications for palaeoclimate reconstructions. Clim. Dyn. 35, 757–770. https://doi.org/10.1007/s00382-009-0616-6.
Gruetzner, J., Matthiessen, J., Geissler, W.H., Gebhardt, A.C., Schreck, M., 2022. A revised core-seismic integration in the Molloy Basin (ODP Site 909): Implications for the history of ice rafting and ocean circulation in the Atlantic-Arctic gateway. Glob. Planet. Chang. 215, 103876. https://doi.org/10.1016/j.gloplacha.2022.103876.
Hall, A.M., Ebert, K., Kleman, J., Nesje, A., Ottesen, D., 2013. Selective glacial erosion on the Norwegian passive margin. Geology 41, 1203–1206. https://doi.org/10.1130/G34806.1.
Hampton, M.A., Lee, H.J., Locat, J., 1996. Submarine landslides. Rev. Geophys. 34, 33–59. https://doi.org/10.1029/95RG03287.
Harbitz, C.B., Løvholt, F., Pedersen, G., Masson, D.G., 2006. Mechanisms of tsunami generation by submarine landslides: a short review. Nor. J. Geol. 86, 255–264.
Harbor, J.M., 1992. Numerical modeling of the development of U-shaped valleys by glacial erosion. Geol. Soc. Am. Bull. 104, 1364–1375. https://doi.org/10.1130/0016-7606(1992)104.
Harishidayat, D., Johansen, S.E., Batchelor, C., Omosanya, K.O., Ottaviani, L., 2021. Pliocene–Pleistocene glacimarine shelf to slope processes in the south-western Barents Sea. Basin Res. 33, 1315–1336. https://doi.org/10.1111/bre.12516.
Haug, G.H., Tiedemann, R., 1998. Effect of the formation of the Isthmus of Panama on Atlantic Ocean thermohaline circulation. Nature 393, 673–676. https://doi.org/10.1038/31447.
Hayashi, T., Yamanaka, T., Hikasa, Y., Sato, M., Kuwahara, Y., Ohno, M., 2020. Latest Pliocene Northern Hemisphere glaciation amplified by intensified Atlantic meridional overturning circulation. Commun. Earth Environ. 1, 1–10. https://doi.org/10.1038/s43247-020-00023-4.
Hijmans, R.J., Cameron, S.E., Parra, J.L., Jones, P.G., Jarvis, A., 2005. Very high resolution interpolated climate surfaces for global land areas. Int. J. Climatol. 25, 1965–1978. https://doi.org/10.1002/joc.1276.
Hill, D.J., 2015. The non-analogue nature of Pliocene temperature gradients. Earth Planet. Sci. Lett. 425, 232–241. https://doi.org/10.1016/j.epsl.2015.05.044.
Hjelstuen, B.O., Sejrup, H.P., 2021. Latitudinal variability in the Quaternary development of the Eurasian ice sheets—evidence from the marine domain. Geology 49, 346–351. https://doi.org/10.1130/G48106.1.
Hjelstuen, B.O., Elverhøi, A., Faleide, J.I., 1996. Cenozoic erosion and sediment yield in the drainage area of the Storfjorden Fan. Glob. Planet. Chang. 12, 95–117. https://doi.org/10.1016/0921-8181(95)00014-3.
Hjelstuen, B.O., Eldholm, O., Faleide, J.I., 2007. Recurrent Pleistocene mega-failures on the SW Barents Sea margin. Earth Planet. Sci. Lett. 258, 605–618. https://doi.org/10.1016/j.epsl.2007.04.025.
Hoff, U., Rasmussen, T.L., Stein, R., Ezat, M.M., Fahl, K., 2016. Sea ice and millennial-scale climate variability in the Nordic seas 90 kyr ago to present. Nat. Commun. 7, 12247. https://doi.org/10.1038/ncomms12247.
Hubbard, A., 2006. The validation and sensitivity of a model of the Icelandic ice sheet. Quat. Sci. Rev. 25, 2297–2313. https://doi.org/10.1016/j.quascirev.2006.04.005.
Hubbard, A., Bradwell, T., Golledge, N., Hall, A., Patton, H., Sugden, D., Cooper, R., Stoker, M., 2009. Dynamic cycles, ice streams and their impact on the extent, chronology and deglaciation of the British–Irish ice sheet. Quat. Sci. Rev. 28, 758–776. https://doi.org/10.1016/j.quascirev.2008.12.026.
Hutchinson, D.K., Coxall, H.K., O'Regan, M., Nilsson, J., Caballero, R., de Boer, A.M., 2019. Arctic closure as a trigger for Atlantic overturning at the Eocene-Oligocene transition. Nat. Commun. 10, 3797. https://doi.org/10.1038/s41467-019-11828-z.
Jakobsson, M., Backman, J., Rudels, B., Nycander, J., Frank, M., Mayer, L., Jokat, W., Sangiorgi, F., O'Regan, M., Brinkhuis, H., King, J., Moran, K., 2007. The early Miocene onset of a ventilated circulation regime in the Arctic Ocean. Nature 447, 986–990. https://doi.org/10.1038/nature05924.
Jamieson, S.S.R., Sugden, D.E., Hulton, N.R.J., 2010. The evolution of the subglacial landscape of Antarctica. Earth Planet. Sci. Lett. 293, 1–27. https://doi.org/10.1016/j.epsl.2010.02.012.
Jansen, E., Sjøholm, J., 1991. Reconstruction of glaciation over the past 6 Myr from ice-borne deposits in the Norwegian Sea. Nature 349, 600–603. https://doi.org/10.1038/349600a0.
Jansen, E., Fronval, T., Rack, F., Channell, J.E.T., 2000. Pliocene-Pleistocene ice rafting history and cyclicity in the Nordic Seas during the last 3.5 Myr. Paleoceanography 15, 709–721. https://doi.org/10.1029/1999PA000435.
Japsen, P., Green, P.F., Bonow, J.M., Nielsen, T.F.D., Chalmers, J.A., 2014. From volcanic plains to glaciated peaks: Burial, uplift and exhumation history of southern East Greenland after opening of the NE Atlantic. Glob. Planet. Chang. 116, 91–114. https://doi.org/10.1016/j.gloplacha.2014.01.012.
Jóhannesson, T., Sigurdsson, O., Laumann, T., Kennett, M., 1995. Degree-day glacier mass-balance modelling with applications to glaciers in Iceland, Norway and Greenland. J. Glaciol. 41, 345–358. https://doi.org/10.3189/S0022143000016221.
Jokat, W., Micksch, U., 2004. Sedimentary structure of the Nansen and Amundsen basins, Arctic Ocean. Geophys. Res. Lett. 31. https://doi.org/10.1029/2003GL018352.
Jungdal-Olesen, G., Andersen, J.L., Born, A., Pedersen, V.K., 2024. The influence of glacial landscape evolution on Scandinavian ice-sheet dynamics and dimensions. Cryosphere 18, 1517–1532. https://doi.org/10.5194/tc-18-1517-2024.
Keigwin, L., 1982. Isotopic Paleoceanography of the Caribbean and East Pacific: Role of Panama Uplift in late Neogene Time. Science 217, 350–353. https://doi.org/10.1126/science.217.4557.350.
Kishankov, A., Serov, P., Bünz, S., Patton, H., Hubbard, A., Mattingsdal, R., Vadakkepuliyambatta, S., Andreassen, K., 2022. Hydrocarbon leakage driven by Quaternary glaciations in the Barents Sea based on 2D basin and petroleum system modeling. Mar. Pet. Geol. 138, 105557. https://doi.org/10.1016/j.marpetgeo.2022.105557.
Kleman, J., Stroeven, A.P., 1997. Preglacial surface remnants and Quaternary glacial regimes in northwestern Sweden. Geomorphology 19, 35–54. https://doi.org/10.1016/S0169-555X(96)00046-3.
Kleman, J., Stroeven, A.P., Lundqvist, J., 2008. Patterns of Quaternary ice sheet erosion and deposition in Fennoscandia and a theoretical framework for explanation. Geomorphology 97, 73–90. https://doi.org/10.1016/j.geomorph.2007.02.049.
Knies, J., Matthiessen, J., Mackensen, A., Stein, R., Vogt, C., Frederichs, T., Nam, S.-I., 2007. Effects of Arctic freshwater forcing on thermohaline circulation during the Pleistocene. Geology 35, 1075. https://doi.org/10.1130/G23966A.1.
Knies, J., Matthiessen, J., Vogt, C., Laberg, J.S., Hjelstuen, B.O., Smelror, M., Larsen, E., Andreassen, K., Eidvin, T., Vorren, T.O., 2009. The Plio-Pleistocene glaciation of the Barents Sea–Svalbard region: a new model based on revised chronostratigraphy. Quat. Sci. Rev. 28, 812–829. https://doi.org/10.1016/j.quascirev.2008.12.002.
Knies, J., Mattingsdal, R., Fabian, K., Grøsfjeld, K., Baranwal, S., Husum, K., De Schepper, S., Vogt, C., Andersen, N., Matthiessen, J., Andreassen, K., Jokat, W., Nam, S.-I., Gaina, C., 2014. Effect of early Pliocene uplift on late Pliocene cooling in the Arctic–Atlantic gateway. Earth Planet. Sci. Lett. 387, 132–144. https://doi.org/10.1016/j.epsl.2013.11.007.
Knudson, K.P., Ravelo, A.C., 2015. North Pacific Intermediate Water circulation enhanced by the closure of the Bering Strait. Paleoceanography 30, 1287–1304. https://doi.org/10.1002/2015PA002840.
Kuvaas, B., Kristoffersen, Y., 1996. Mass movements in glaciomarine sediments on the Barents Sea continental slope. In: Global and Planetary Change, Impact of Glaciations on Basin Evolution: Data and Models from the Norwegian Margin and Adjacent Areas, 12, pp. 287–307. https://doi.org/10.1016/0921-8181(95)00025-9.
Laberg, J.S., Vorren, T.O., 1993. A late Pleistocene submarine slide on the Bear Island Trough Mouth Fan. Geo-Mar. Lett. 13, 227–234. https://doi.org/10.1007/BF01207752.
Laberg, J.S., Vorren, T.O., 2000. The Trænadjupet Slide, offshore Norway — morphology, evacuation and triggering mechanisms. Mar. Geol. 171, 95–114. https://doi.org/10.1016/S0025-3227(00)00112-2.
Laberg, J.S., Vorren, T.O., Dowdeswell, J.A., Kenyon, N.H., Taylor, J., 2000. The Andøya Slide and the Andøya Canyon, north-eastern Norwegian–Greenland Sea. Mar. Geol. 162, 259–275. https://doi.org/10.1016/S0025-3227(99)00087-0.
Laberg, J.S., Eilertsen, R.S., Vorren, T.O., 2009. The paleo–ice stream in Vestfjorden, North Norway, over the last 35 k.y.: Glacial erosion and sediment yield. Geol. Soc. Am. Bull. 121, 434–447. https://doi.org/10.1130/B26277.1.
Laberg, J.S., Andreassen, K., Knies, J., Vorren, T.O., Winsborrow, M., 2010. Late Pliocene-Pleistocene development of the Barents Sea Ice Sheet. Geology 38, 107–110. https://doi.org/10.1130/G30193.1.
Laberg, J.S., Andreassen, K., Vorren, T.O., 2012. Late Cenozoic erosion of the high-latitude southwestern Barents Sea shelf revisited. Geol. Soc. Am. Bull. 124, 77–88. https://doi.org/10.1130/B30340.1.
Lasabuda, A., Geissler, W.H., Laberg, J.S., Knutsen, S.-M., Rydningen, T.A., Berglar, K., 2018a. Late Cenozoic Erosion estimates for the Northern Barents Sea: Quantifying Glacial Sediment Input to the Arctic Ocean. Geochem. Geophys. Geosyst. 19, 4876–4903. https://doi.org/10.1029/2018GC007882.
Lasabuda, A., Laberg, J.S., Knutsen, S.-M., Safronova, P., 2018b. Cenozoic tectonostratigraphy and pre-glacial erosion: a mass-balance study of the

northwestern Barents Sea margin, Norwegian Arctic. J. Geodyn. 119, 149–166. https://doi.org/10.1016/j.jog.2018.03.004.
Lasabuda, A.P.E., Johansen, N.S., Laberg, J.S., Faleide, J.I., Senger, K., Rydningen, T.A., Patton, H., Knutsen, S.-M., Hanssen, A., 2021. Cenozoic uplift and erosion of the Norwegian Barents Shelf – a review. Earth Sci. Rev. 217, 103609. https://doi.org/10.1016/j.earscirev.2021.103609.
Lasabuda, A.P.E., Hanssen, A., Laberg, J.S., Faleide, J.I., Patton, H., Abdelmalak, M.M., Rydningen, T.A., Kjølhamar, B., 2023. Paleobathymetric reconstructions of the SW Barents Seaway and their implications for Atlantic–Arctic ocean circulation. Commun. Earth Environ. 4, 1–17. https://doi.org/10.1038/s43247-023-00899-y.
Laumann, T., Reeh, N., 1993. Sensitivity to climate-change of the mass-balance of glaciers in southern Norway. J. Glaciol. 39, 656–665. https://doi.org/10.3189/S0022143000016555.
Le Meur, E., Huybrechts, P., 1996. A comparison of different ways of dealing with isostasy: examples from modeling the Antarctic ice sheet during the last glacial cycle. Ann. Glaciol. 23, 309–317. https://doi.org/10.3189/S0260305500013586.
Leynaud, D., Mienert, J., Vanneste, M., 2009. Submarine mass movements on glaciated and non-glaciated European continental margins: a review of triggering mechanisms and preconditions to failure. Mar. Pet. Geol. 26, 618–632. https://doi.org/10.1016/j.marpetgeo.2008.02.008.
Liakka, J., Löfverström, M., Colleoni, F., 2016. The impact of the north American glacial topography on the evolution of the Eurasian ice sheet over the last glacial cycle. Clim. Past 12, 1225–1241. https://doi.org/10.5194/cp-12-1225-2016.
Lien, Ø.F., Hjelstuen, B.O., Zhang, X., Sejrup, H.P., 2022. Late Plio-Pleistocene evolution of the Eurasian Ice Sheets inferred from sediment input along the northeastern Atlantic continental margin. Quat. Sci. Rev. 282, 107433. https://doi.org/10.1016/j.quascirev.2022.107433.
Lisiecki, L.E., Raymo, M.E., 2005. A Pliocene-Pleistocene stack of 57 globally distributed benthic δ18O records. Paleoceanography 20, PA1003. https://doi.org/10.1029/2004PA001071.
Llopart, J., Urgeles, R., Camerlenghi, A., Lucchi, R.G., Rebesco, M., De Mol, B., 2015. Late Quaternary development of the Storfjorden and Kveithola Trough Mouth fans, northwestern Barents Sea. Quat. Sci. Rev. 129, 68–84. https://doi.org/10.1016/j.quascirev.2015.10.002.
Løseth, H., Lippard, S.J., Sættem, J., Fanavoll, S., Fjerdingstad, V., Leith, T.L., Ritter, U., Smelror, M., Sylta, O., Vorren, T.O., 1993. Cenozoic uplift and erosion of the Barents Sea — Evidence from the Svalis Dome area. In: Bergsager, E., Dahl-Stamnes, Ø.A., Holter, E., Johansen, B., Lie, E., Lund, T.B. (Eds.), Norwegian Petroleum Society Special Publications. Elsevier, pp. 643–664. https://doi.org/10.1016/B978-0-444-88943-0.50042-3.
Løtveit, I.F., Fjeldskaar, W., Sydnes, M., 2019. Tilting and Flexural Stresses in Basins due to Glaciations—an example from the Barents Sea. Geosciences 9, 474. https://doi.org/10.3390/geosciences9110474.
Luckman, A., Benn, D.I., Cottier, F., Bevan, S., Nilsen, F., Inall, M., 2015. Calving rates at tidewater glaciers vary strongly with ocean temperature. Nat. Commun. 6, 8566. https://doi.org/10.1038/ncomms9566.
Lunt, D.J., Foster, G.L., Haywood, A.M., Stone, E.J., 2008. Late Pliocene Greenland glaciation controlled by a decline in atmospheric CO_2 levels. Nature 454, 1102–1105. https://doi.org/10.1038/nature07223.
MacGregor, K.R., Anderson, R.S., Anderson, S.P., Waddington, E.D., 2000. Numerical simulations of glacial-valley longitudinal profile evolution. Geology 28, 1031–1034. https://doi.org/10.1130/0091-7613(2000)28<1031:NSOGLP>2.0.CO;2.
Martínez-Botí, M.A., Foster, G.L., Chalk, T.B., Rohling, E.J., Sexton, P.F., Lunt, D.J., Pancost, R.D., Badger, M.P.S., Schmidt, D.N., 2015. Plio-Pleistocene climate sensitivity evaluated using high-resolution CO_2 records. Nature 518, 49–54. https://doi.org/10.1038/nature14145.
Maslin, M.A., Li, X.S., Loutre, M.-F., Berger, A., 1998. The contribution of orbital forcing to the progressive intensification of northern hemisphere glaciation. Quat. Sci. Rev. 17, 411–426. https://doi.org/10.1016/S0277-3791(97)00047-4.
Mattingsdal, R., Knies, J., Andreassen, K., Fabian, K., Husum, K., Grøsfjeld, K., De Schepper, S., 2014. A new 6 Myr stratigraphic framework for the Atlantic–Arctic Gateway. Quat. Sci. Rev. 92, 170–178. https://doi.org/10.1016/j.quascirev.2013.08.022.
McClymont, E.L., Ho, S.L., Ford, H.L., Bailey, I., Berke, M.A., Bolton, C.T., De Schepper, S., Grant, G.R., Groeneveld, J., Inglis, G.N., Karas, C., Patterson, M.O., Swann, G.E.A., Thirumalai, K., White, S.M., Alonso-Garcia, M., Anand, P., Hoogakker, B.A.A., Littler, K., Petrick, B.F., Risebrobakken, B., Abell, J.T., Crocker, A.J., de Graaf, F., Feakins, S.J., Hargreaves, J.C., Jones, C.L., Markowska, M., Ratnayake, A.S., Stepanek, C., Tangunan, D., 2023. Climate evolution through the onset and intensification of Northern Hemisphere Glaciation. Rev. Geophys. 61, e2022RG000793. https://doi.org/10.1029/2022RG000793.
Medvedev, S., Hartz, E.H., Podladchikov, Y.Y., 2008. Vertical motions of the fjord regions of central East Greenland: Impact of glacial erosion, deposition, and isostasy. Geology 36, 539–542. https://doi.org/10.1130/G24638A.1.
Medvedev, S., Hartz, E.H., Faleide, J.I., 2018. Erosion-driven vertical motions of the circum Arctic: Comparative analysis of modern topography. J. Geodyn. 119, 62–81. https://doi.org/10.1016/j.jog.2018.04.003.
Medvedev, S., Faleide, J.I., Hartz, E.H., 2023. Cenozoic reshaping of the Barents-Kara Shelf: Influence of erosion, sedimentation, and glaciation. Geomorphology 420, 108500. https://doi.org/10.1016/j.geomorph.2022.108500.
Mienert, J., Vanneste, M., Bünz, S., Andreassen, K., Haflidason, H., Sejrup, H.P., 2005. Ocean warming and gas hydrate stability on the mid-Norwegian margin at the Storegga Slide. Mar. Pet. Geol. 22, 233–244. https://doi.org/10.1016/j.marpetgeo.2004.10.018.
Miller, K.G., Browning, J.V., Schmelz, W.J., Kopp, R.E., Mountain, G.S., Wright, J.D., 2020. Cenozoic Sea-level and cryospheric evolution from deep-sea geochemical and continental margin records. Sci. Adv. 6, eaaz1346. https://doi.org/10.1126/sciadv.aaz1346.
Montelli, A., Dowdeswell, J.A., Ottesen, D., Johansen, S.E., 2017. Ice-sheet dynamics through the Quaternary on the mid-Norwegian continental margin inferred from 3D seismic data. Mar. Pet. Geol. 80, 228–242. https://doi.org/10.1016/j.marpetgeo.2016.12.002.
Montgomery, D.R., Balco, G., Willett, S.D., 2001. Climate, tectonics, and the morphology of the Andes. Geology 29, 579–582. https://doi.org/10.1130/0091-7613(2001)029<0579:CTATMO>2.0.CO;2.
Mudelsee, M., Raymo, M.E., 2005. Slow dynamics of the Northern Hemisphere glaciation. Paleoceanography 20. https://doi.org/10.1029/2005PA001153.
Nikishin, A.M., Gaina, C., Petrov, E.I., Malyshev, N.A., Freiman, S.I., 2018. Eurasia Basin and Gakkel Ridge, Arctic Ocean: Crustal asymmetry, ultra-slow spreading and continental rifting revealed by new seismic data. Tectonophysics 746, 64–82. https://doi.org/10.1016/j.tecto.2017.09.006.
O'Dea, A., Lessios, H.A., Coates, A.G., Eytan, R.I., Restrepo-Moreno, S.A., Cione, A.L., Collins, L.S., de Queiroz, A., Farris, D.W., Norris, R.D., Stallard, R.F., Woodburne, M.O., Aguilera, O., Aubry, M.-P., Berggren, W.A., Budd, A.F., Cozzuol, M.A., Coppard, S.E., Duque-Caro, H., Finnegan, S., Gasparini, G.M., Grossman, E.L., Johnson, K.G., Keigwin, L.D., Knowlton, N., Leigh, E.G., Leonard-Pingel, J.S., Marko, P.B., Pyenson, N.D., Rachello-Dolmen, P.G., Soibelzon, E., Soibelzon, L., Todd, J.A., Vermeij, G.J., Jackson, J.B.C., 2016. Formation of the Isthmus of Panama. Sci. Adv. 2, e1600883. https://doi.org/10.1126/sciadv.1600883.
Öğretmen, N., Schiebel, R., Jochum, K.P., Stoll, B., Weis, U., Repschläger, J., Jentzen, A., Galer, S., Haug, G.H., 2020. Deep Thermohaline Circulation across the Closure of the central American Seaway. Paleoceanogr. Paleoclimatol. 35, e2020PA004049. https://doi.org/10.1029/2020PA004049.
Patton, H., Hubbard, A., Andreassen, K., Winsborrow, M., Stroeven, A.P., 2016a. The build-up, configuration, and dynamical sensitivity of the Eurasian ice-sheet complex to late Weichselian climatic and oceanic forcing. Quat. Sci. Rev. 153, 97–121. https://doi.org/10.1016/j.quascirev.2016.10.009.
Patton, H., Swift, D.A., Clark, C.D., Livingstone, S.J., Cook, S.J., 2016b. Distribution and characteristics of overdeepenings beneath the Greenland and Antarctic ice sheets: Implications for overdeepening origin and evolution. Quat. Sci. Rev. 148, 128–145. https://doi.org/10.1016/j.quascirev.2016.07.012.
Patton, H., Hubbard, A., Andreassen, K., Auriac, A., Whitehouse, P., Stroeven, A.P., Shackleton, C., Winsborrow, M.C.M., Heyman, J., Hall, A.M., 2017a. Deglaciation of the Eurasian ice sheet complex. Quat. Sci. Rev. 169, 148–172. https://doi.org/10.1016/j.quascirev.2017.05.019.
Patton, H., Hubbard, A., Bradwell, T., Schomacker, A., 2017b. The configuration, sensitivity and rapid retreat of the late Weichselian Icelandic ice sheet. Earth Sci. Rev. 166, 223–245. https://doi.org/10.1016/j.earscirev.2017.02.001.
Patton, H., Hubbard, A., Heyman, J., Alexandropoulou, N., Lasabuda, A.P.E., Stroeven, A.P., Hall, A.M., Winsborrow, M., Sugden, D.E., Kleman, J., Andreassen, K., 2022. The extreme yet transient nature of glacial erosion. Nat. Commun. 13, 7377. https://doi.org/10.1038/s41467-022-35072-0.
Petrov, O., Morozov, A., Shokalsky, S., Kashubin, S., Artemieva, I.M., Sobolev, N., Petrov, E., Ernst, R.E., Sergeev, S., Smelror, M., 2016. Crustal structure and tectonic model of the Arctic region. Earth Sci. Rev. 154, 29–71. https://doi.org/10.1016/j.earscirev.2015.11.013.
Piasecka, E.D., Winsborrow, M.C.M., Andreassen, K., Stokes, C.R., 2016. Reconstructing the retreat dynamics of the Bjørnøyrenna Ice Stream based on new 3D seismic data from the Central Barents Sea. Quat. Sci. Rev. 151, 212–227. https://doi.org/10.1016/j.quascirev.2016.09.003.
Pollard, D., DeConto, R.M., 2007. A coupled ice-sheet/ice-shelf/sediment model applied to a marine-margin flowline: forced and unforced variations. In: Hambrey, M.J., Christoffersen, P., Glasser, N.F., Hubbard, B. (Eds.), Glacial Sedimentary Processes and Products. John Wiley & Sons, Ltd, Oxford, pp. 37–52. https://doi.org/10.1002/9781444304435.ch4.
Pope, E.L., Talling, P.J., Carter, L., 2017. Which earthquakes trigger damaging submarine mass movements: Insights from a global record of submarine cable breaks?. In: Marine Geology, Subaquatic Paleoseismology: Records of Large Holocene Earthquakes in Marine and Lacustrine Sediments, 384, pp. 131–146. https://doi.org/10.1016/j.margeo.2016.01.009.
Pope, E.L., Talling, P.J., Cofaigh, C., 2018. The relationship between ice sheets and submarine mass movements in the Nordic Seas during the Quaternary. Earth Sci. Rev. 178, 208–256. https://doi.org/10.1016/j.earscirev.2018.01.007.
Rabassa, J., Clapperton, C.M., 1990. Quaternary glaciations of the southern Andes. Quat. Sci. Rev. 9, 153–174. https://doi.org/10.1016/0277-3791(90)90016-4.
Rasmussen, E., Fjeldskaar, W., 1996. Quantification of the Pliocene-Pleistocene erosion of the Barents Sea from present-day bathymetry. Glob. Planet. Chang. 12, 119–133. https://doi.org/10.1016/0921-8181(95)00015-1.
Raymo, M.E., 1994. The Initiation of Northern Hemisphere Glaciation. Annu. Rev. Earth Planet. Sci. 22, 353–383. https://doi.org/10.1146/annurev.ea.22.050194.002033.
Raymo, M.E., Ruddiman, W.F., 1992. Tectonic forcing of late Cenozoic climate. Nature 359, 117–122. https://doi.org/10.1038/359117a0.
Raymo, M.E., Ruddiman, W.F., Backman, J., Clement, B.M., Martinson, D.G., 1989. Late Pliocene variation in northern hemisphere ice sheets and North Atlantic deep water circulation. Paleoceanography 4, 413–446. https://doi.org/10.1029/PA004i004p00413.
Rebesco, M., Wåhlin, A., Laberg, J.S., Schauer, U., Beszczynska-Möller, A., Lucchi, R.G., Noormets, R., Accettella, D., Zarayskaya, Y., Diviacco, P., 2013. Quaternary contourite drifts of the Western Spitsbergen margin. Deep-Sea Res. I Oceanogr. Res. Pap. 79, 156–168. https://doi.org/10.1016/j.dsr.2013.05.013.
Rebesco, M., Laberg, J.S., Pedrosa, M.T., Camerlenghi, A., Lucchi, R.G., Zgur, F., Wardell, N., 2014. Onset and growth of Trough-Mouth fans on the North-Western

Barents Sea margin – implications for the evolution of the Barents Sea/Svalbard Ice Sheet. Quat. Sci. Rev. 92, 227–234. https://doi.org/10.1016/j.quascirev.2013.08.015.

Riis, F., Fjeldskaar, W., 1992. On the magnitude of the late Tertiary and Quaternary erosion and its significance for the uplift of Scandinavia and the Barents Sea. In: Larsen, R.M., Brekke, H., Larsen, B.T., Talleraas, E. (Eds.), Structural and Tectonic Modelling and its Application to Petroleum Geology. Norwegian Petroleum Society Special Publications. Elsevier, Amsterdam, pp. 163–185. https://doi.org/10.1016/B978-0-444-88607-1.50016-4.

Rise, L., Ottesen, D., Longva, O., Solheim, A., Andersen, E.S., Ayers, S., 2006. The Sklinnadjupet slide and its relation to the Elsterian glaciation on the mid-Norwegian margin. Mar. Pet. Geol. 23, 569–583. https://doi.org/10.1016/j.marpetgeo.2006.05.005.

Ruddiman, W.F., Raymo, M.E., 1988. Northern Hemisphere climate regimes during the past 3 Ma: possible tectonic connections. Philos. Trans. R. Soc. B 318, 411–430. https://doi.org/10.1098/rstb.1988.0017.

Rudels, B., Korhonen, M., Schauer, U., Pisarev, S., Rabe, B., Wisotzki, A., 2015. Circulation and transformation of Atlantic water in the Eurasian Basin and the contribution of the Fram Strait inflow branch to the Arctic Ocean heat budget. Progr. Oceanogr. Oceanogr. Arctic North Atlantic Basins 132, 128–152. https://doi.org/10.1016/j.pocean.2014.04.003.

Rydningen, T.A., Høgseth, G.V., Lasabuda, A.P.E., Laberg, J.S., Safronova, P.A., Forwick, M., 2020. An early Neogene—early Quaternary Contourite Drift System on the SW Barents Sea Continental margin, Norwegian Arctic. Geochem. Geophys. Geosyst. 21, e2020GC009142. https://doi.org/10.1029/2020GC009142.

Sættem, J., Poole, D.A.R., Ellingsen, L., Sejrup, H.P., 1992. Glacial geology of outer Bjørnøyrenna, southwestern Barents Sea. Mar. Geol. 103, 15–51. https://doi.org/10.1016/0025-3227(92)90007-5.

Safronova, P.A., Laberg, J.S., Andreassen, K., Shlykova, V., Vorren, T.O., Chernikov, S., 2017. Late Pliocene–early Pleistocene deep-sea basin sedimentation at high-latitudes: mega-scale submarine slides of the North-Western Barents Sea margin prior to the shelf-edge glaciations. Basin Res. 29, 537–555. https://doi.org/10.1111/bre.12161.

Schoof, C., 2007. Marine ice-sheet dynamics. Part 1. The case of rapid sliding. J. Fluid Mech. 573, 27. https://doi.org/10.1017/S0022112006003570.

Seguinot, J., 2013. Spatial and seasonal effects of temperature variability in a positive degree-day glacier surface mass-balance model. J. Glaciol. 59, 1202–1204. https://doi.org/10.3189/2013JoG13J081.

Seki, O., Foster, G.L., Schmidt, D.N., Mackensen, A., Kawamura, K., Pancost, R.D., 2010. Alkenone and boron-based Pliocene pCO_2 records. Earth Planet. Sci. Lett. 292, 201–211. https://doi.org/10.1016/j.epsl.2010.01.037.

Serov, P., Mattingsdal, R., Winsborrow, M., Patton, H., Andreassen, K., 2023. Widespread natural methane and oil leakage from sub-marine Arctic reservoirs. Nat. Commun. 14, 1782. https://doi.org/10.1038/s41467-023-37514-9.

Serov, P., Andreassen, K., Winsborrow, M., Mattingsdal, R., Patton, H., 2024. Geological and glaciological controls of 21,700 active methane seeps in the northern Norwegian Barents Sea. Front. Earth Sci. 12. https://doi.org/10.3389/feart.2024.1404027.

Singer, B.S., Ackert, R.P., Guillou, H., 2004. $^{40}Ar/^{39}Ar$ and K-Ar chronology of Pleistocene glaciations in Patagonia. Geol. Soc. Am. Bull. 116, 434–450. https://doi.org/10.1130/B25177.1.

Solheim, A., Kristoffersen, Y., 1984. The Physical Environment in the Western Barents Sea, 1: 5,000,000. Sediments above the Upper Regional Unconformity: Thickness, Seismic Stratigraphy and Outline of the Glacial History. Norsk Polarinstitutt.

Steer, P., Huismans, R.S., Valla, P.G., Gac, S., Herman, F., 2012. Bimodal plio-quaternary glacial erosion of fjords and low-relief surfaces in Scandinavia. Nat. Geosci. 5, 635–639. https://doi.org/10.1038/ngeo1549.

Stein, R., Fahl, K., 2013. Biomarker proxy shows potential for studying the entire Quaternary Arctic Sea ice history. Org. Geochem. 55, 98–102. https://doi.org/10.1016/j.orggeochem.2012.11.005.

Stein, R., Stax, R., 1996. 22. Organic carbon and N-Alkane distribution in late Cenozoic sediments of Arctic gateways sites 909 and 911 and their paleoenvironmental implications: Preliminary results. In: Thiede, J., Myhre, A.M., Firth, J.V., Johnson, G. L., Ruddiman, W.F. (Eds.), Proceedings of the Ocean Drilling Program, Scientific Results. Ocean Drilling Program. https://doi.org/10.2973/odp.proc.sr.151.1996.

Straume, E.O., Nummelin, A., Gaina, C., Nisancioglu, K.H., 2022. Climate transition at the Eocene–Oligocene influenced by bathymetric changes to the Atlantic–Arctic oceanic gateways. Proc. Natl. Acad. Sci. 119, e2115346119. https://doi.org/10.1073/pnas.2115346119.

Struijk, E.L.M., Tesauro, M., Lebedeva-Ivanova, N.N., Gaina, C., Beekman, F., Cloetingh, S.A.P.L., 2018. The Arctic lithosphere: Thermo-mechanical structure and effective elastic thickness. In: Global and Planetary Change, From the Deep Earth to the Surface, 171, pp. 2–17. https://doi.org/10.1016/j.gloplacha.2018.07.014.

Sugden, D.E., 1978. Glacial Erosion by the Laurentide Ice Sheet. J. Glaciol. 20, 367–391. https://doi.org/10.3189/S0022143000013915.

Svendsen, J.I., Alexanderson, H., Astakhov, V.I., Demidov, I., Dowdeswell, J.A., Funder, S., Gataullin, V., Henriksen, M., Hjort, C., Houmark-Nielsen, M., Hubberten, H.W., Ingólfsson, Ó., Jakobsson, M., Kjær, K.H., Larsen, E., Lokrantz, H., Lunkka, J.P., Lyså, A., Mangerud, J., Matiouchkov, A., Murray, A., Möller, P., Niessen, F., Nikolskaya, O., Polyak, L., Saarnisto, M., Siegert, C., Siegert, M.J., Spielhagen, R.F., Stein, R., 2004. Late Quaternary ice sheet history of northern Eurasia. Quat. Sci. Rev. 23, 1229–1271. https://doi.org/10.1016/j.quascirev.2003.12.008.

Tomkin, J.H., Braun, J., 2002. The influence of alpine glaciation on the relief of tectonically active mountain belts. Am. J. Sci. 302, 169–190. https://doi.org/10.2475/ajs.302.3.169.

van der Veen, C.J., 2002. Polar ice sheets and global sea level: how well can we predict the future? Glob. Planet. Chang. 32, 165–194. https://doi.org/10.1016/S0921-8181(01)00140-0.

van der Veen, C.J., 2013. Fundamentals of Glacier Dynamics. A.A. Balkema, Rotterdam. https://doi.org/10.1201/b14059.

Vorren, T.O., Laberg, J.S., 1997. Trough mouth fans — palaeoclimate and ice-sheet monitors. Quat. Sci. Rev. 16, 865–881. https://doi.org/10.1016/S0277-3791(97)00003-6.

Vorren, T.O., Lebesbye, E., Andreassen, K., Larsen, K.-B., 1989. Glacigenic sediments on a passive continental margin as exemplified by the Barents Sea. Mar. Geol. 85, 251–272. https://doi.org/10.1016/0025-3227(89)90156-4.

Vorren, T.O., Richardsen, G., Knutsen, S.-M., Henriksen, E., 1991. Cenozoic erosion and sedimentation in the western Barents Sea. Mar. Pet. Geol. 8, 317–340. https://doi.org/10.1016/0264-8172(91)90086-G.

Waage, M., Bünz, S., Bøe, R., Mienert, J., 2018. High-resolution 3D seismic exhibits new insights into the middle-late Pleistocene stratigraphic evolution and sedimentary processes of the Bear Island trough mouth fan. Mar. Geol. 403, 139–149. https://doi.org/10.1016/J.MARGEO.2018.05.006.

Wickert, A.D., 2016. Open-source modular solutions for flexural isostasy: gFlex v1.0. Geosci. Model Dev. 9, 997–1017. https://doi.org/10.5194/gmd-9-997-2016.

Willeit, M., Ganopolski, A., Calov, R., Brovkin, V., 2019. Mid-Pleistocene transition in glacial cycles explained by declining CO_2 and regolith removal. Sci. Adv. 5, eaav7337. https://doi.org/10.1126/sciadv.aav7337.

Winkelmann, D., Stein, R., 2007. Triggering of the Hinlopen/Yermak Megaslide in relation to paleoceanography and climate history of the continental margin north of Spitsbergen. Geochem. Geophys. Geosyst. 8. https://doi.org/10.1029/2006GC001485.

Wu, J., Mollenhauer, G., Stein, R., Köhler, P., Hefter, J., Fahl, K., Grotheer, H., Wei, B., Nam, S.-I., 2022. Deglacial release of petrogenic and permafrost carbon from the Canadian Arctic impacting the carbon cycle. Nat. Commun. 13, 7172. https://doi.org/10.1038/s41467-022-34725-4.

Zieba, K.J., Felix, M., Knies, J., 2016. The Pleistocene contribution to the net erosion and sedimentary conditions in the outer Bear Island Trough, western Barents Sea. arktos 2, 23. https://doi.org/10.1007/s41063-016-0022-3.

Zieba, K.J., Omosanya, K.O., Knies, J., 2017. A flexural isostasy model for the Pleistocene evolution of the Barents Sea bathymetry. Nor. J. Geol. 97, 1–19. https://doi.org/10.17850/njg97-1-01.